

Construction of detrital mineral populations: insights from mixing of U–Pb zircon ages in Himalayan rivers

William H. Amidon,* Douglas W. Burbank* and George E. Gehrels†

*Department of Geological Sciences, University of California, Santa Barbara, CA, USA

†Department of Geosciences, University of Arizona, Tucson, AZ, USA

ABSTRACT

Fission-track, U–Pb and Pb–Pb analyses of detrital heavy mineral populations in depositional basins and modern river sediments are widely used to infer the exhumational history of mountain belts. However, relatively few studies address the underlying assumption that detrital mineral populations provide an accurate representation of their entire source region. Implicit in this assumption is the idea that all units have equal potential to contribute heavy minerals in proportion to their exposure area in the source region. In reality, the detrital mineral population may be biased by variable concentrations of minerals in bedrock and differential erosion rates within the source region. This study evaluates the relative importance of these two variables by using mixing of U–Pb zircon ages to trace zircon populations from source units, through the fluvial system, and into the foreland.

The first part of the study focuses on the Marsyandi drainage in central Nepal, using tributaries that drain single formations to define the U–Pb age distributions of individual units and using trunk river samples to evaluate the relative contributions from each lithology. Observed mixing proportions are compared with proportions predicted by a simple model incorporating lithologic exposure area and zircon concentration. The relative erosion rates that account for the discrepancy between the observed and predicted mixing proportions are then modelled and compared with independent erosional proxies. The study also compares U–Pb age distributions from four adjacent drainages spanning ~250 km along the Himalayan front using the Kolmogorov–Smirnov statistic and statistical estimates of the proportion of zircon derived from each upstream lithology. Results show that, along this broad swath of rugged mountains, the U–Pb age distributions are remarkably similar, thereby allowing data from more localized sources to be extrapolated along strike.

INTRODUCTION

During the erosion of large fold–thrust belts, eroded sediment is deposited in adjacent foreland basins, thereby preserving a detrital record of orogenic growth. Because of their durability and diagnostic occurrence in source rocks, detrital heavy mineral assemblages in foreland sediments have long been used to assess relative contributions from source units or terranes. More recently, the advancement of single-grain geochronologic techniques has allowed the use of detrital mineral ages as a tool to determine mineral provenance, as well as to gain valuable information about the thermal and exhumational conditions of the source region.

Despite the widespread application of heavy mineral analysis in fields ranging from plate tectonics to geomorphology, the controls on the ways in which foreland heavy mineral assemblages are constructed have not been thoroughly investigated. When a detrital sample is stated to represent the source area, this implicitly assumes that the

proportion of detrital minerals derived from a specific lithology is proportional to its exposure area.

Using zircon as an example, this study addresses the importance of three fundamental variables in construction of the foreland mineral population: exposure area of a given source lithology, heterogeneous distribution of heavy minerals in source rock and variable erosion rates within the source area. Lithologic exposure areas are determined in ArcGIS using digitized geologic maps overlaid on a 90-m digital elevation model (DEM). Variability in zircon concentration and grain size is assessed in bedrock and river sediment by applying our newly developed technique of separating, photographing, counting and dimensioning individual zircon grains to estimate the total number of grains per mass of sediment (Amidon *et al.*, 2005).

We then use U–Pb zircon ages from 15 samples of modern river sediment in the Marsyandi drainage of central Nepal to trace zircons from specific source units within the Himalaya through the fluvial system and into the foreland. The U–Pb zircon-age signature of each source unit is assessed through samples of tributary catchments dominated by single units, whereas trunk-river samples reflect the relative importance of contributions from each unit. The relative contributions of zircon from each unit are then

Correspondence: William H. Amidon, Geological and Planetary Sciences Division, California Institute of Technology, Pasadena, CA 91125, USA. E-mail: wamidon@gps.caltech.edu

calculated by iterative and inverse statistical techniques introduced in Amidon *et al.* (2005). These techniques evaluate the proportions in which multiple component age distributions have combined to create a mixed age distribution.

A simple model is then constructed in which the observed zircon mixing proportions are compared with the mixing proportions predicted based on the relative exposure area and estimated zircon concentration of each unit. To evaluate the importance of differential erosion rates, we forward model the relative erosion rates that would create a match between the observed and predicted mixing proportions and compare them with published precipitation and erosional data. Results show that in the Marsyandi catchment, higher zircon concentrations in the upper-half of the drainage offset apparently higher erosion rates in the lower-half to create an observed age distribution that is a reasonable match with that predicted by exposure area alone. However, we show that despite accounting for up to 12% of the drainage area, a granitic lithology contributes no detectable zircon to the fluvial system. This result confirms that detrital mineral populations may inadequately represent certain parts of the landscape as suggested by Spiegel *et al.* (2004).

The second part of the study compares U–Pb zircon age distributions from four adjacent drainages spanning ~250 km along the Himalayan front in central Nepal, and a fifth sample downstream of their confluence. Age distributions for each sample were compared using the Kolmogorov–Smirnov (KS) test to evaluate the spatial homogeneity of ages contributed from different regions of the mountain range. Additionally, the relative proportions of each contributing unit were estimated for all five samples, and compared with predictions based on exposure area and concentration of each unit. Results from the four large drainages along the Himalayan front suggest that the composition of the detrital population is sensitive to the effects of erosion rate and zircon concentration, but that because these variables are fairly constant on the scale of ~250 km, they do not create strong variations between adjacent drainages in the Nepal Himalaya.

THE IMPORTANCE OF MINERAL CONCENTRATION, EROSION RATE AND GRAIN SIZE IN DETRITAL STUDIES

The recent increase in studies utilizing detrital heavy minerals has been accompanied by few studies that address potential biases in the detrital population (Morton & Smale, 1991; Morton & Johnsson, 1993; Morton & Hallsworth, 1999; Garzanti *et al.*, 2004; Spiegel *et al.*, 2004). Before presenting our results, we discuss the importance of heavy mineral concentration in bedrock and differential erosion rates and how they have been addressed in previous detrital studies. Although our study focuses on zircon, we broaden our discussion to include apatite and monazite because they share similar properties and are likely to occur and behave in ways analogous to zircon.

A review of previous studies indicates that, whereas relative abundances of heavy minerals are often used to constrain provenance, variations in absolute concentration are rarely defined (Hubert, 1971; Turnau–Morawska, 1984; Morton, 1985; Morton & Hallsworth, 1994; Lihou & Mange–Rajetzky, 1996). However, intuition and petrologic literature suggest that there are strong variations in absolute mineral concentrations. For example, igneous rocks of mafic to intermediate composition contain little or no zircon, apatite or monazite and thus contribute nothing to the detrital population (Gromet & Silver, 1983; Cullers & Graf, 1984; Frey, 1984). In contrast, alkaline and calc-alkaline compositions, such as granite, consistently host these minerals in modal abundances <0.1% (Poldervaart, 1956; Poitrasson *et al.*, 2002). Higher concentrations of heavy minerals are found in late-stage intrusives such as carbonatitic dikes in southern Malawi and the soil column above them, which average ~10 and ~5.6% monazite, respectively (Holt, 1965). Although such rock types are extremely uncommon, their high heavy mineral concentration means that even a spatially limited occurrence could still contribute the majority of heavy minerals to a fluvial system.

Sedimentary and meta-sedimentary rocks often contain higher heavy mineral concentrations than any igneous rock, and are much more common. Because of their durability and density, zircon and monazite are long-lived minerals that become concentrated into placer deposits in high-energy environments, such as rivers and near-shore marine facies (Rubey, 1933; Rittenhouse, 1943; Slingerland, 1984, 1997). For example, zircon and monazite occur as trace minerals in sands of the Nile River, but become concentrated to 13.6 and 7.3%, respectively, in deltaic placers (Frihy *et al.*, 1995). Placer deposits off the southern Indian coast contain as much as 80% heavy minerals with ~5% monazite (Karve *et al.*, 1966). The frequent occurrence of placer deposits in marine sediments and sedimentary rocks suggests they are the primary source of heavy minerals to fluvial systems in drainages with sedimentary bedrock (Overstreet, 1967; Jones & Davies, 1979; Shideler & Flores, 1980; Neary & Highley, 1984; Day & Fletcher, 1991; Behera, 2003; Surour *et al.*, 2003).

Accordingly, concentrations of heavy minerals are expected to vary on the orogen scale. Smale (1990) reviewed the distribution of heavy minerals on the South Island of New Zealand, revealing that zircon and apatite occur in high concentrations in some isolated regions and are non-existent in other areas. This implies that detrital mineral populations from terrestrial basins on the South Island are dominated by grains from distinct 'point sources' in the landscape, rather than representing a spatially integrated sample. Similarly, Spiegel *et al.* (2004) found that the non-contribution of detrital zircons from basic magmatic lithologies strongly biased the detrital mineral population towards other parts of the drainage. Thus, it is important to assess lithologic constraints on the source of heavy minerals before conducting a detrital study.

The contribution of grains from distinct source regions may also be biased by differential erosion rates between

regions. For example, erosion rates estimated by sediment flux in Taiwan range over an order of magnitude from < 1 to $> 20 \text{ mm yr}^{-1}$ within the same drainage basin (Dadson *et al.*, 2003). Estimates of erosion on $\sim 1 \text{ Myr}$ time scales based on apatite U–Th/He ages from the Cascade Range exhibit approximately six-fold differences ranging from 0.05 to 0.3 mm yr^{-1} within the same catchment (Reiners *et al.*, 2003). As a result, it cannot be assumed that each part of a drainage is eroding at the same rate, and thus contributing the same number of heavy minerals to the detrital population. Garver *et al.* (1999) addressed this problem in their approach to using detrital fission-track grain age distributions to estimate the proportion of the Indus drainage that is eroding at different rates. They divided each probability value in the probability density age plot by its associated erosion rate and then renormalized the plot to an area of one, such that the size of age peaks is not biased by erosion rate. However, when applying single-grain geochemical techniques (U–Pb, Pb–Pb, trace element analysis, etc.) that are insensitive to the exhumational history of the grain, independent estimates of erosion rate in the source region should be considered.

Grain size, morphology and other physical characteristics are also important considerations in detrital thermochronology because they strongly affect a grain's hydraulic properties and its likelihood of being sampled for analysis. Variations in grain size and morphology are common in sedimentary rocks, where they are a function of the sediment supply and hydraulic energy of the depositional environment. Thus, natural energy variations create biases in the grain-size distribution of both sedimentary source rocks, and in the sediments or sedimentary rocks from which the minerals are eventually sampled. The importance of this bias is magnified by the fact that most geochronologic techniques require reasonably large ($> 50 \mu\text{m}$) non-metamict grains with relatively few fractures or inclusions (Dickinson & Gehrels, 2003; Ehlers & Farley, 2003; Bernet *et al.*, 2004).

GEOLOGIC BACKGROUND

Structural history of the central Nepal Himalaya

Following initial collision of India and Asia $\sim 55 \text{ Ma}$, sedimentary rocks of the northern Indian margin were stacked in a series of south-vergent thrust sheets (Gansser, 1964; Hodges, 2000). The structurally highest rocks are a sequence of Cambrian to Jurassic limestones, sandstones and shales known as the Tethyan Sedimentary Series (Figs 2 and 3). The base of the Tethyan Series is marked by a family of north-dipping, normal-sense shear zones known as the South Tibetan Detachment (STD) (Hodges *et al.*, 1996; Searle & Godin, 2003). Below the STD lies the Greater Himalayan Series, a continuous sequence of amphibolite-grade schists and gneisses divided from south to north into Formations I–III (Le Fort, 1975; Searle & Godin, 2003). Formation III is augen gneiss, probably re-

presenting Paleozoic intrusions or volcanoclastic horizons in the calc-silicate rocks of Formation II (Colchen *et al.*, 1986; Hodges *et al.*, 1996; Gehrels *et al.*, 2003) (Fig. 1). Despite their higher grade and structural separation, it has been proposed that the calcic gneisses of Formation II are correlative with the Annapurna Yellow and Nilgiri formations that constitute the basal units of the Tethyan Series (Fig. 2) (Le Fort, 1975; Gehrels *et al.*, 2003). Down section to the south, Formation II transitions into the pelitic gneisses of Formation I, which are in turn bounded by the Main Central Thrust (MCT) at their base (Searle & Godin, 2003; Hodges *et al.*, 2004).

The MCT is traditionally mapped as a laterally continuous zone of sheared rocks separating the Greater Himalayan Series in its hanging wall from the lower-grade schists and meta-sediments of the Lesser Himalayan Series in its footwall (Hodges, 2000; Pearson & DeCelles, 2005; Martin *et al.*, 2005). Previous workers have proposed MCT activity between the late Oligocene and mid-Miocene (Coleman *et al.*, 1996; Grujic *et al.*, 2002; Searle & Godin, 2003), with activity beginning on the Main Boundary Thrust (MBT) during the Pliocene (DeCelles *et al.*, 1998, 2001). The MBT defines the contact between the Lesser Himalayan rocks in its hanging wall and thick packages of Neogene fluvial sedimentary rocks known as the Siwalik group in its footwall (DeCelles *et al.*, 1998; Upreti, 1999). Farther to the south, the Main Frontal Thrust (MFT) places the Siwalik group against Quaternary foreland basin deposits (Powers *et al.*, 1998; Lavé and Avouac, 2000; DeCelles *et al.*, 2001).

Tectonics, sedimentation and U–Pb zircon ages

Detailed understanding of the structure of the Nepal Himalaya is hindered in part by a limited understanding of the depositional relationships between the major meta-sedimentary units. All of the major lithotectonic units originated on the northern margin of India prior to its collision with Asia, but the exact sediment sources and depositional geometries remain vague. Existing constraints are based largely on observed variations in U–Pb zircon age distributions. For example, most Lesser Himalaya units do not contain zircon ages younger than $\sim 1600 \text{ Ma}$ and are characterized by a multi-peaked cluster of ages between 1800 and 2000 Ma (DeCelles *et al.*, 1998, 2000, 2004; Gehrels *et al.*, 2003; Martin *et al.*, 2005). Greater Himalayan rocks contain ages as young as $\sim 490 \text{ Ma}$, with clusters of ages between 800 and 1000 Ma , and between 2400 and 2600 Ma (Fig. 3). Cambrian–Jurassic strata of the Tethyan Himalaya contain an almost identical age spectrum to that of the Greater Himalaya, but also include abundant 470 – 500 Ma ages (Gehrels *et al.*, 2003; Martin *et al.*, 2005). Martin *et al.* (2005) presented data from five transects spanning $\sim 150 \text{ km}$ along strike in the central Nepal Himalaya. When compared with data from Amidon *et al.* (2005), the Greater Himalayan age distributions appear similar at all sites, although there are noticeably fewer ages $> 1200 \text{ Ma}$ in the

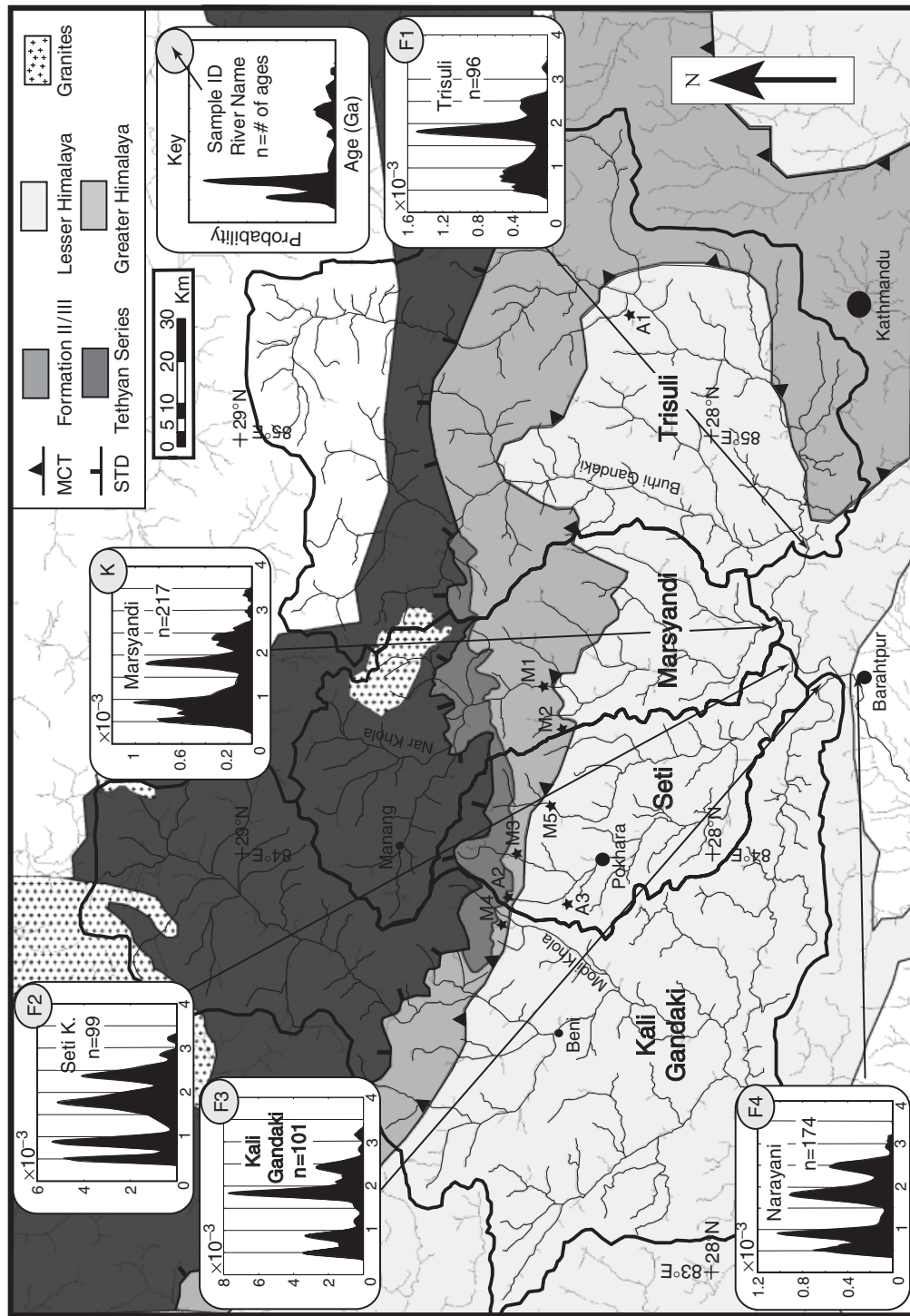


Fig. 1. Simplified geologic map of the study area compiled from Searle & Godin (2003), Colchen *et al.* (1986) and Fuchs (1980). The South Tibetan Detachment (STD) and Main Central Thrust (MCT) are displayed in their original locations as mapped by Colchen *et al.* (1986). Locations of geologic features outside of the Marsyandi drainage may not be precise because they were digitized from a 1 : 500 000 scale map. Drainage areas are delineated by heavy black lines and U–Pb zircon age distributions are shown for samples from four adjacent drainages, and from the Narayani river downstream of their confluence. Locations of bedrock U–Pb zircon samples displayed in Fig. 3 are displayed as stars.

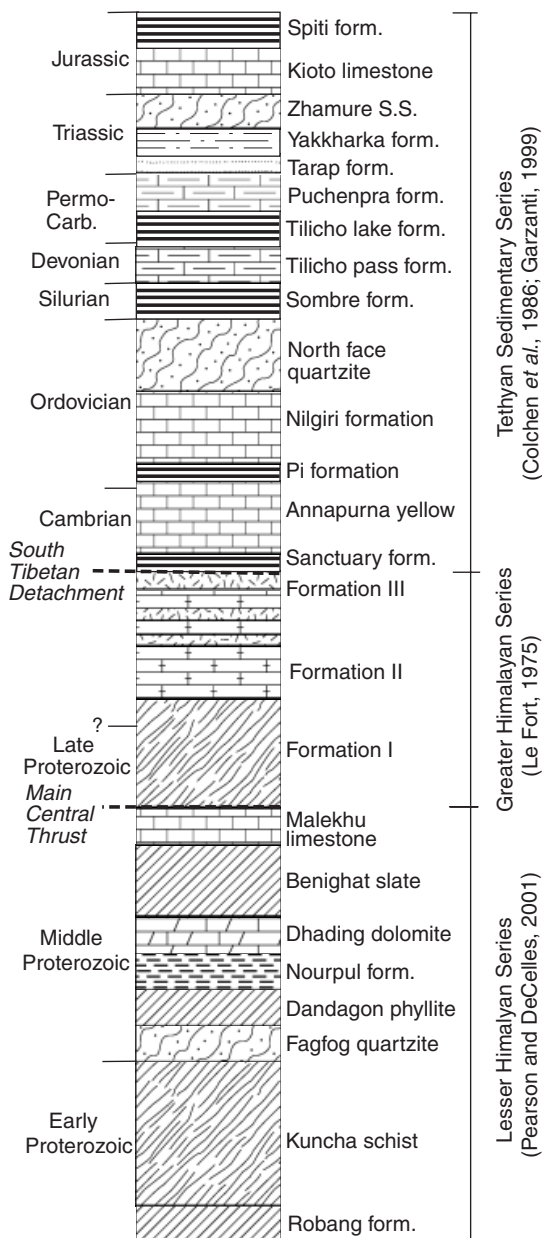


Fig. 2. Highly schematic stratigraphic column for central Nepal. Relative thicknesses displayed in the figure may not reflect actual unit thicknesses. Le Fort (1975) proposed correlation of Formation II with the lowermost Tethyan Sedimentary Series between the Sanctuary and Nilgiri formations.

two westernmost distributions (Fig. 3). The Lesser Himalayan distributions are also consistent despite variations in age frequencies attributable to different analytical errors. Thus, it appears that U–Pb age distributions are consistent on the scale of hundreds of kilometres and can be used to fingerprint units in central Nepal.

METHODS

Sampling locations

The first part of our study focuses on the Marsyandi drainage, where six modern sand samples (A, C, D, F, H and I)

were taken from small tributaries to define the contribution from specific formations (Fig. 4). Additionally, four sand samples were taken from the Marsyandi River where it crosses the STD (B), the Formation I–II contact (E), the MCT (G) and just above the confluence with the Trisuli River (K). These samples were deliberately taken just downstream of where the Marsyandi crosses formational boundaries and were used to determine the proportion of zircon contributed from each of the upstream formations. One additional sand sample was taken from the Darondi Khola (J) to evaluate the proportions of zircon derived from the Greater and Lesser Himalaya with no contribution from the Tethyan Series.

The second part of our study focuses on comparisons between the age distributions of detrital zircons from four adjacent drainage basins along the Himalayan front. From east to west, these drainages are the Trisuli (F1), including the Burhi Gandaki, the Marsyandi (K), the Seti (F2) and the Kali Gandaki (F3). A fifth sample was taken from the Narayani River (F4) below the confluence of rivers represented by the previous four samples (Fig. 1).

Field and laboratory methods

Each sample consists of 10–15 ‘grab’ samples taken from deposits of coarse to very coarse sand on large bars that represent the active channel bed during high flow and are only exposed during low water stands. Samples for U–Pb analysis were concentrated in the field using a gold pan, with final zircon separation in the laboratory by standard density and magnetic techniques. Samples for estimating zircon concentration in river sediments were separated only using Methelyne Iodide (density 3.3 g cm^{-3}), and a frantz magnetic separator with a final pass of 1.8 A , 8° tilt and 15° slope. No water table step was used during separation. Random aliquots were selected from the resulting heavy mineral concentrates, mounted on epoxy disks parallel to their C-axis and polished to $\sim 1/2$ the thickness of the smaller grains. Grain mount maps and CL images were generated using a scanning electron microscope. The isotopes ^{238}U , ^{232}Th , ^{208}Pb , ^{207}Pb , ^{206}Pb and ^{204}Pb were measured simultaneously by LA-MC-ICPMS, which is critical to this study because it (1) avoids biasing the sample by hand picking, (2) allows random analysis of mounted grains by moving along a pre-determined grid (excluding heavily metamict or fractured grains), (3) allows analysis of zircon cores instead of the entire grain for large grains and (4) allows rapid inexpensive analysis of numerous grains.

Analyses were performed for ~ 20 s each, excavating a crater $\sim 20 \mu\text{m}$ in depth using a $50\text{-}\mu\text{m}$ diameter laser spot size. Separate ages were calculated from the measured $^{238}\text{U}/^{206}\text{Pb}$ and $^{207}\text{Pb}/^{206}\text{Pb}$ ratios for every grain. If the average of the two calculated ages was $< 1 \text{ Ga}$, the $^{238}\text{U}/^{206}\text{Pb}$ age was used; otherwise, the $^{207}\text{Pb}/^{206}\text{Pb}$ age was used. All grain ages from a given sample were included in the sample age distribution unless the total grain-age error on an individual grain was $> 20\%$ or the analysis was $> 20\%$ discordant or $> 10\%$ reverse discordant. In

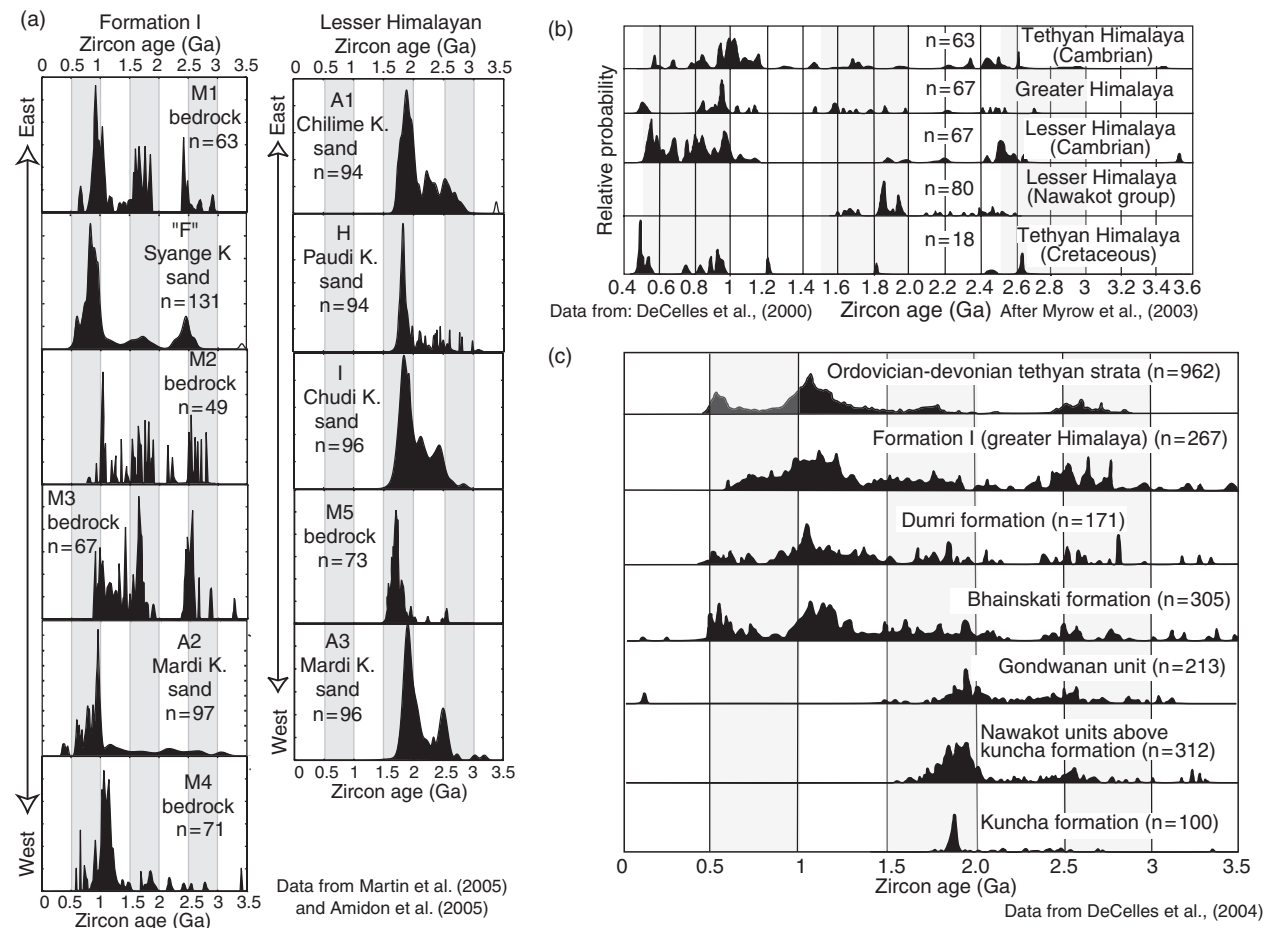


Fig. 3. Published U–Pb age distributions from the Himalaya. Panel A shows samples of bedrock U–Pb ages from Martin *et al.* (2005), whose sample number begins with ‘M’, and ages from Amidon *et al.* (2005) from mono-lithologic drainages, whose sample numbers begin with ‘A’. Sample locations are shown in Fig. 1. Note that the peak positions between ~800 and 1200 Ma may be slightly offset between the two sets of age distributions because Martin *et al.* (2005) use $^{207}\text{Pb}/^{206}\text{Pb}$ ages for average ages > 800 Ma while Amidon *et al.* (2005) use $^{207}\text{Pb}/^{206}\text{Pb}$ for ages > 1000 Ma. Panel B shows bedrock U–Pb zircon ages from Cambrian units of the Lesser and Tethyan Himalaya in India from Myrow *et al.* (2003). Ages from the Greater Himalayan, Lesser Himalayan (Nawakot Group) and Tethyan Himalaya (Cretaceous) of Nepal are from DeCelles *et al.* (2000). Panel C shows bedrock U–Pb zircon age distributions constructed from very large sample sizes for a range of formations in Nepal, published in DeCelles *et al.* (2004).

all cases, 1σ errors are used, typically between 4 and 10%, which include measurement error, ^{204}Pb correction error and fractionation correction error. Detailed instrumental and analytical procedures followed those of Dickinson & Gehrels (2003).

Concentration and grain-size analysis

To assess the variability in zircon concentration between formations, we measured the concentration of zircon in seven samples of river sediment and six bedrock samples (locations shown in Fig. 1). Bulk samples were weighed, the grain-size distribution of river sands was determined (Table 1) and all zircons were separated without using any hydraulic separation steps. If the heavy mineral concentrate was too large to count in full, three aliquots were randomly taken from each sample and weighed. The aliquots were digitally photographed and imported into the graphics program Canvas where all grains were counted and ~200–400 grains per sample were measured. The total

number of zircons in the aliquots was used to estimate the total number of zircons in the sample, thereby allowing an estimate of concentration in units of total zircon grains per initial sample mass (Tables 2 and 3). Grain measurements also allow an estimate of the proportion of grains that are < 60 μm in width, and thus the concentration of grains that were actually dated in this study (Tables 2 and 3). The overall reliability of this technique has been verified in Amidon *et al.* (2005) by comparing concentration estimates obtained from grain counting with those obtained by measuring bulk Zr in river sediments: results between the two techniques agree to within ± 10%.

Determining lithologic exposure area

The exposure area and average hill slope angle for each formation within a given drainage basin were determined in ArcGIS using a digitized geologic map overlaid on a 3-arc-sec (90-m) DEM. A composite geologic map was created from the maps of Searle & Godin (2003), Colchen *et al.*

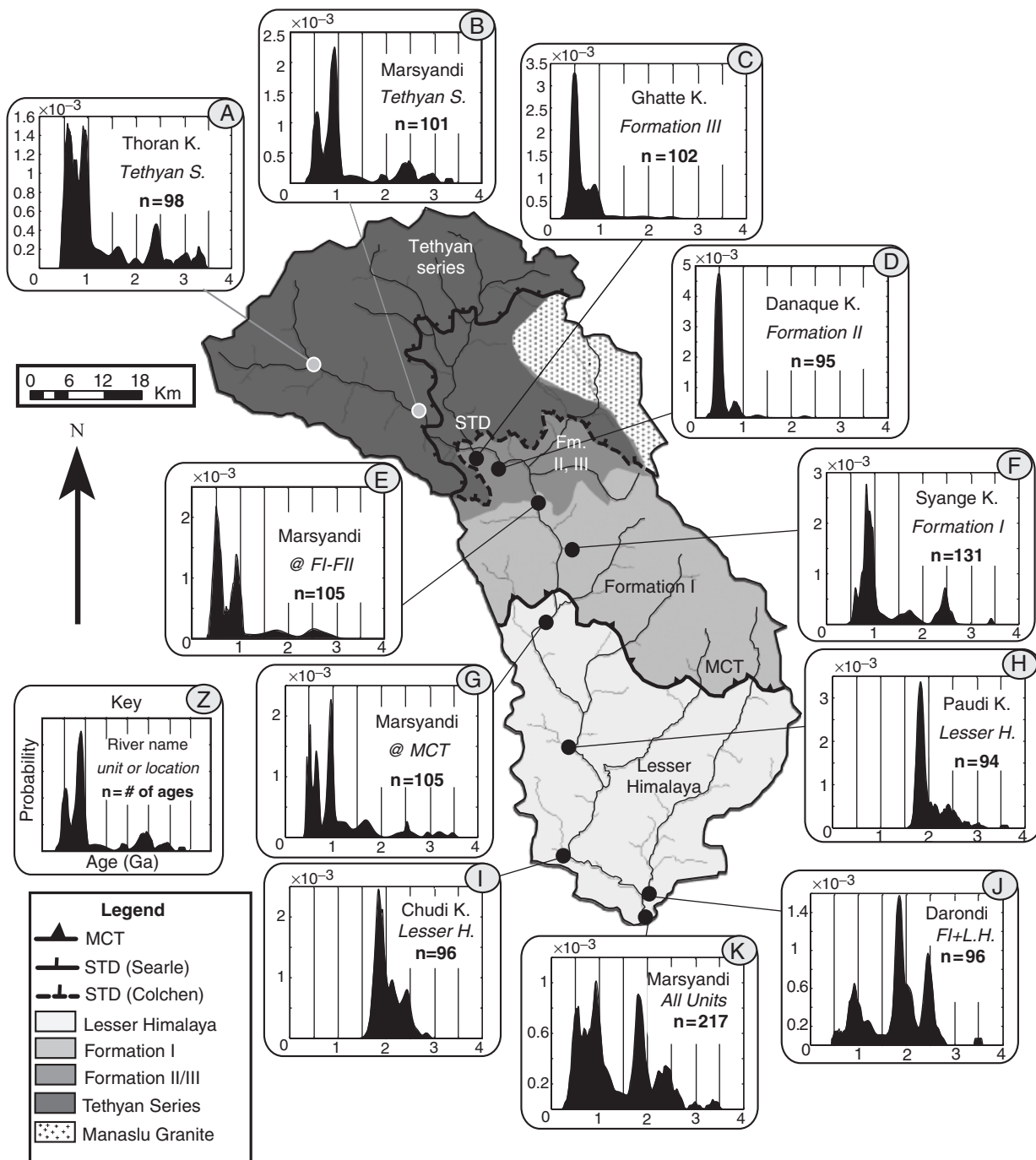


Fig. 4. Geologic map of the Marsyandi drainage, central Nepal digitized from the combined maps of Searle & Godin (2003) and Colchen *et al.* (1986). Solid lines represent the Main Central Thrust and South Tibetan Detachment (STD) as mapped by Searle & Godin (2003). The dashed line is the STD as mapped by Colchen *et al.* (1986). U–Pb zircon age distributions are shown for samples of river sediment taken from either tributaries draining single geologic units (A, C, D, F, H and I) or the main stem Marsyandi (B, E, G and K).

(1986) and Fuchs (1980), with priority given in that order where features were inconsistent between maps (Fig. 4). Such a combination of maps was necessary because the oldest map was too large in scale and lacked sufficient detail in the Marsyandi region, while the younger two were not spatially extensive enough to cover the entire field area. As a result, the locations of features within the Marsyandi drainage are highly accurate, whereas some uncertainty exists regarding the exact location of contacts elsewhere on

the map area. In particular, the map may not depict the entire extent of Formations II and III in the western portion of the map, and does not differentiate between units of the Tethyan Series.

Calculating observed mixing of U–Pb ages

Age distributions for each sample are expressed as probability density functions (PDFs) in which all of the

Table 1. Grain size distribution of sediment samples used to define zircon concentration (shown as proportion of total sample mass)

Phi	-2	-1	0	1	2	3	4	5+
(mm)	>4	>2	>1	>0.5	>0.25	>0.125	>0.63	<0.63
TSS-1 (B)	0.00	0.01	0.05	0.25	0.39	0.16	0.09	0.05
TSS-2 (Nar)	0.05	0.06	0.10	0.25	0.34	0.14	0.05	0.01
FII-1 (D)	0.03	0.03	0.11	0.30	0.34	0.13	0.04	0.01
FI-1 (F)	0.04	0.05	0.11	0.28	0.32	0.12	0.06	0.01
LHS-2 (H)	0.00	0.00	0.02	0.19	0.43	0.19	0.12	0.04
LHS-1 (I)	0.02	0.04	0.10	0.37	0.34	0.08	0.03	0.01
TSS-unused	0.00	0.00	0.02	0.08	0.26	0.35	0.21	0.08

measured ages and their associated Gaussian errors are summed and normalized to a total probability of 1 (Eqn. (1)):

$$P(x) = \sum_{i=1}^N (1/2\sigma_i\sqrt{2\pi})e^{-(x-\mu_i)^2/2\sigma_i^2} \quad (1)$$

where σ_i is the 1σ grain-age error, μ_i is the mean grain age and x a given age value (Myr).

The proportion in which two or more PDFs combine to create a downstream mixed PDF is determined by both an iterative and an inverse approach. Both techniques rely on the basic relationship:

$$\phi_a P(A) + \phi_b P(B) + (1 - \phi_a - \phi_b)P(C) = P(D) \quad (2)$$

where $P(A)$, $P(B)$ and $P(C)$ are component PDFs that have mixed in some unknown proportions ϕ_a , ϕ_b and $(1 - \phi_a - \phi_b)$ to create a downstream mixed PDF, $P(D)$. This relationship is constrained by the fact that both ϕ_a and ϕ_b must be positive decimals where $(\phi_a + \phi_b) \leq 1$. Two fundamental assumptions must be met to satisfy Eqn. (2): (1) the downstream mixed PDF, $P(D)$, must be a finite mixture of only the component PDFs $P(A)$, $P(B)$ and $P(C)$ and (2) all of the sample PDFs must be accurate representations of their true underlying age distributions.

In reality, the second assumption is often violated because of the difficulty in representing a complex underlying age distribution with ~ 100 grain ages. This issue was addressed in Amidon *et al.* (2005) by creating two 'parent' populations from >450 lesser and greater Himalayan zircon ages. We then used Monte Carlo subsampling to determine the ideal smoothing interval, which, when applied to subsampled PDFs, created the best match between the subsample and parent PDFs (Fig. 5). Based on the results of this experiment, we smooth all sample PDFs with an 80-Myr window prior to performing any mixing calculations.

The iterative approach to determine the proportion of each component PDF present in a downstream mixed PDF combines the component PDFs in every possible combination of ϕ values until the resulting artificial mixed PDF has the lowest percent area mismatch (Eqn. (3)) with

the observed mixed PDF:

$$\left(\left(\sum_{i=1}^N |artificial - observed| \right) / 2 \right) \times 100 \quad (3)$$

The set of ϕ values that yields the lowest mismatch estimates the proportion of zircons derived from the formations represented by each PDF.

The inverse mixing approach uses a constrained least-squares inversion to estimate the proportion of each component PDF in the mixed PDF. This relies on the fact that if the above assumptions hold true, then the equality in Eqn. (1) should be satisfied at every age increment (1, 2, 3, ..., 4000 Ma). Because all of the component PDFs and the mixed PDFs are known, a least-squares inversion can effectively solve for the mixing parameters ϕ_a , ϕ_b and $(1 - \phi_a - \phi_b)$ that minimize the sum of the squared differences between the two sides of Eqn. (1) at every age increment. This approach involves expressing the probability values in each PDF in vector form (each PDF has 4000 discrete probability values corresponding to each age increment), rewriting Eqn. (1) in vector form $Ax = B$ and inverting to solve for x . A more detailed treatment of the constrained least-squares inversion used in this study is given in Menke (1989) and in Amidon *et al.* (2005), where we deal extensively with the accuracy and robustness of these two approaches to estimate mixing proportions. Based on Monte Carlo simulations using artificially mixed Himalayan age distributions, we show that both techniques provide consistently accurate estimates of ϕ to within ± 0.06 over a range of ϕ values (Amidon *et al.*, 2005). Excellent agreement between the two techniques when applied to the mixing estimates in this study further justify their application to estimates of PDF mixing. In cases where the two techniques yield differing estimates (never more than 0.02), we have used the inverse estimate.

Mixing predictions and modelled erosion rates

For each main-stem sample location that allows calculation of the relative proportion of zircons derived from each formation, a prediction was made of the relative proportions of zircon expected based on lithologic exposure area

Table 2. Results of zircon counting in bedrock samples

Geologic unit and sample number	1	2	3	4	5	6	7	8	9	10	11	12	13
	Avg. length (µm)	Avg. width (µm)	% Euhedral	% Fragment	% Ellipsoid	% Round	Estimated # of zircons in sample	% > 60 µm	Estimated # of zircons > 60 mm in sample	Bulk weight (g)	Conc. (grains g ⁻¹)	Conc. > 60 µm (grains g ⁻¹)	Average conc. of aliquots
TSS-1 (qtzte)	75	44	4	32	49	15	5538	8	443	950	5.83	0.47	N/A
TSS-2 (qtzte)	89	46	11	42	41	6	17450	10	1745	800	21.81	2.18	N/A
TSS-3 (qtzte)	120	67	8	30	46	16	8709	65	5661	1014	8.59	5.58	N/A
TSS-4 (qtzte)	109	65	15	35	38	12	15089	64	9657	1157	13.04	8.35	N/A
FII-1	155	71	6	77	16	0	43	78	34	1343	0.03	0.03	N/A
FII-2A	90	53	33	67	0	0	178	54	96	1014	0.18	0.10	0.10
FII-2B	103	58	24	39	34	3	255	39	101	1014	0.25	0.10	
FI-1A	145	85	3	31	62	4	22438	96	21594	1184	18.95	18.24	18.66
FI-1B	147	86	5	27	59	8	23471	96	22585	1184	19.82	19.07	
FI-2A	114	74	10	32	45	13	6440	71	4577	1458	4.42	3.14	3.05
FI-2B	112	74	5	33	51	11	4634	93	4320	1458	3.18	2.96	
FI-3	91	49	8	22	65	5	373521	12	45196	693	538.99	65.22	N/A
FI-4	104	52	2	40	54	4	4382	17	745	736	5.95	1.01	N/A
LHS-1A	176	93	27	23	42	7	5439	97	5303	800	6.80	6.63	N/A
LHS-1B	190	100	10	38	51	1	5232	100	5232	800	6.54	6.54	6.68
LHS-1C	183	96	9	41	49	1	5918	93	5490	800	7.40	6.86	
LHS-2	144	89	4	42	53	1	391	96	375	1114	0.35	0.34	N/A
M.G.-1	136	54	40	60	0	0	10	100	10	1250	0.008	0.008	N/A
M.G.-2	142	62	60	40	0	0	5	100	5	729	0.007	0.0069	N/A
M.G.-3	113	46	80	20	0	0	5	100	5	857	0.006	0.0058	N/A
M.G.-4	138	62	50	50	0	0	4	100	4	943	0.004	0.0042	N/A
M.G.-5	122	51	60	40	0	0	10	100	10	986	0.010	0.0101	N/A

Avg., average; Conc., concentration; N/A, not applicable.

Table 3. Results of zircon counting in river sediments draining single geologic units

Geologic unit and sample number	1	2	3	4	5	6	7	8	9	10	11	12	13
	Avg. length (µm)	Avg. width (µm)	% Euh.	% Frag.	% Egg	% Rnd.	Estimated # of zircons in sample	% > 60 µm	Estimated # of zircons > 60 µm in sample	Bulk weight (g)	Conc. (grains g ⁻¹)	Conc. > 60 µm (grains g ⁻¹)	Average conc. of aliquots
TSS-1A (B)	154.0	91.0	4	43	51	3	4600	89.5	4116	702	6.55	5.86	5.60
TSS-1B (B)	159.0	92.5	2	33	64	2	3897	96.1	3746	702	5.55	5.34	
TSS-(Nar)	140.0	97.0	14	34	35	11	2337	94.1	2199	558	4.18	3.94	3.94
FI-1 (D)	185.0	103.5	29	29	31	7	766	86.9	666	802	0.96	0.83	0.83
FI-1A (F)	170.2	95.6	4	39	53	3	7940	68.6	5448	897	8.85	6.07	6.48
FI-1B (F)	165.2	91.7	5	31	60	5	6217	92.7	5763	897	6.93	6.42	
FI-1C (F)	151.7	88.8	2	46	51	1	8954	69.4	6216	897	9.98	6.93	
LHS-2 (H)	184.0	102.0	24	42	31	3	903	89.9	812	504	1.79	1.61	1.61
LHS-1A (I)	156.2	82.5	11	41	47	1	3240	80.3	2601	895	3.62	2.91	2.66
LHS-1B (I)	167.3	86.3	7	33	58	1	2310	93.4	2157	895	2.58	2.41	
<i>Zircon counting statistics on the < 300 µm size fraction, not on bulk sediments (from Amidon et al., 2005)</i>													
A1 (GHS)	136.5	90.0	48	30	13	9	N/A	N/A	22997	377	N/A	61.00	N/A
A2 (GHS)	168.5	113.6	28	37	20	15	N/A	N/A	5040	180	N/A	58.00	N/A
A1 (LHS)	140.9	97.6	20	14	45	21	N/A	N/A	3132	54	N/A	28.00	N/A
A2 (LHS)	152.0	104.8	21	34	30	15	N/A	N/A	1586	122	N/A	13.00	N/A

Avg., average; Conc., concentration; N/A, not applicable.

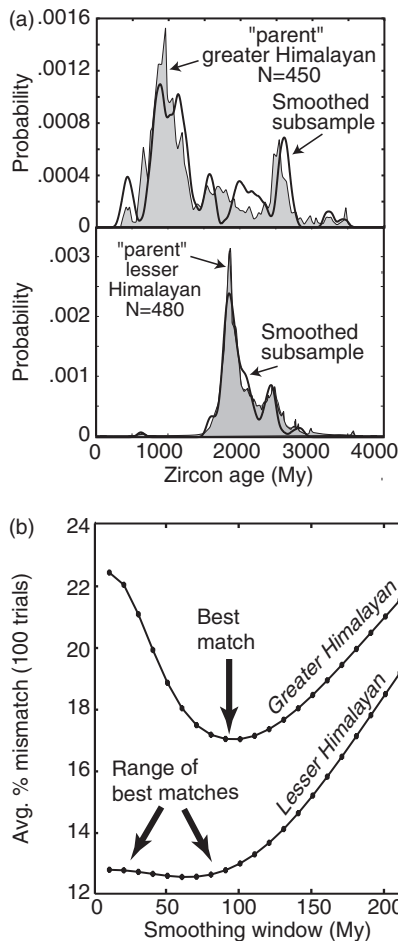
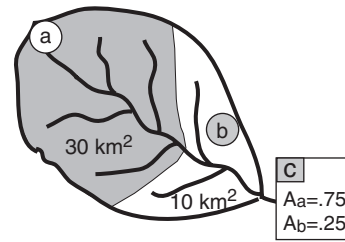


Fig. 5. Figure from Amidon *et al.* (2005) showing the results of an experiment designed to determine the degree of subsample smoothing that yields the best match between parent and subsample. Monte Carlo subsampling was used to draw 100 grain subsamples from two Himalayan 'parent' distributions constructed from the data of Gehrels *et al.* (2003) and Amidon *et al.* (2005). After smoothing the subsamples, the percent area mismatch was determined between parent and subsample. Average mismatch was determined over 100 trials for each successively larger smoothing window. Results show that smoothing all data with a window of ~80 Myr will provide an optimal match for both Greater and Lesser Himalayan age distributions.

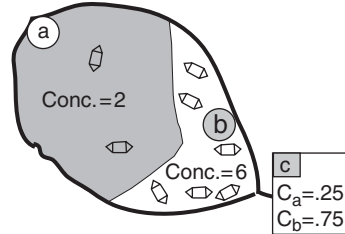
and zircon concentration. These predictions rely on a simple model in which two separate initial predictions are made: one based on the relative exposure areas of each formation within a given drainage, and a second based on the relative concentrations of zircon in each formation in the drainage. The area and concentration predictions for each formation in a given drainage are then multiplied together and renormalized by the summed products for all formations in the drainage. The resulting proportions are a combined prediction based on exposure area and zircon concentration as described in Fig. 6.

The predicted mixing proportions for each sample typically differ from the observed mixing proportions at the same site. Some of this discrepancy is because of differential erosion rates between different formations.

(a) Area prediction:



(b) Concentration prediction:



(c) Combined prediction:

1	$A_a * C_a = .1875$ $A_b * C_b = .1875$
2	$(A_a * C_a) / [(A_b * C_b) + (A_a * C_a)] = .5$ $(A_b * C_b) / [(A_b * C_b) + (A_a * C_a)] = .5$
3	Predicted mixing proportion: 1a:1b

(d) Observed mixing of U-Pb ages:

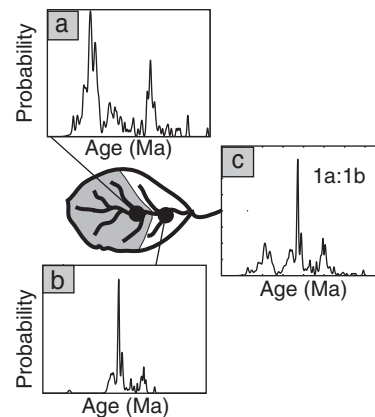


Fig. 6. This figure illustrates the simple model used to predict the proportion of zircon derived from each upstream lithology. First, separate predictions of the zircon mixing proportions based on lithologic exposure area and relative zircon concentration are made (panels A and B). The two predicted proportions for each lithology in the drainage are then multiplied (step 1; panel C) and divided by their summed products (step 2; panel C), which yields the combined predicted proportions based on both lithologic exposure area and relative zircon concentration (step 3; panel C). Predicted zircon mixing proportions are then compared with proportions observed in the actual mixed downstream sample (bottom panel).

However, because formation-specific erosion rates are unknown, they are not included in the predictive model. Instead, we use the combined area–concentration prediction to forward model the formation-specific relative erosion rates that would create the best match with the observed mixing proportions. The predicted erosion rates are then compared with published erosion rates from the Himalaya to assess the model.

The KS test

To quantify differences among PDFs from the four adjacent drainages and the downstream mixed sample, we performed the KS test on paired PDFs from different drainages. This non-parametric statistical test determines whether observed differences between data distributions are more than would be expected from random chance (Press, 1997; Sheskin, 2003). This test is useful for comparing detrital age distributions because it makes no assumptions about how the data are distributed and is thus sensitive to both the position of age peaks and the shape of the overall probability curve (Berry *et al.*, 2001; DeGraaf-Surpless *et al.*, 2003). Depending upon the combined sample size, the KS statistic corresponds to a probability value (*P*) representing the probability that differences between the two distributions are not more than would be expected based on random chance (Table 7).

ANALYSIS AND RESULTS

Initial observations

Age distributions from the Marsyandi drainage show clear downstream trends reflecting the input of zircons from successive formations (Fig. 4). Sample B characterizes the age distribution of the Marsyandi as it emerges from post-Ordovician Tethyan units. The trunk river then receives contributions from Formations II and III, which, based on their similarity, are treated as a single source in mixing calculations. Downstream of Formation II, sample E contains a large proportion of ages < 700 Ma and a relative paucity of ages > 1000 Ma, suggesting a larger contribution from Formation II/III than would be expected based on its limited exposure area (Fig. 4 and Table 4). Further downstream, sample G shows a strong peak between 900 and 1000 Ma, and more ages > 1000 Ma indicating a moderate, but not dominant, contribution from Formation I (sample F; Fig. 4).

Samples H and I (Fig. 4) characterize Lesser Himalayan age distributions that are in excellent agreement with previously reported ages shown in Fig. 3 (DeCelles *et al.*, 2000; Martin *et al.*, 2005). The contribution of Lesser Himalayan zircons is clear in sample K (Fig. 4) from the lowest Marsyandi, which contains large peaks at ~1800 and 2400 Ma. The importance of the Tethyan Series and Formation II/III contributions to sample K is apparent in the high age probability between ~480 and 700 Ma. This interpretation is confirmed by comparison with sample J, which

Table 4. Lithologic exposure area and average hillslope angle for individual lithologies in the Marsyandi drainage

Tethyan series post-Ordovician		Tethyan series Ordovician		Miocene granite		Formation II/III		Formation I (above F)		Formation I (above K)		Lesser Himalaya		Total area (km ²)							
km ²	%	km ²	%	km ²	%	km ²	%	km ²	%	km ²	%	km ²	%								
1996	40.0	31	556	11.2	37.2	278	5.6	37	257	5.2	359	459	9.2	35.4	1069	21.4	33.6	1440	28.9	23.7	4986

Avg., average.

contains no Tethyan or Formation II/III ages and lacks significant age probability between ~ 480 and 700 Ma. Sample J also has a prominent peak at ~ 1 Ga derived from Formation I. A much larger ~ 1 Ga peak in sample K reflects a Formation I source combined with a significant contribution of ~ 1 Ga ages from the Tethyan series.

The distributions of the Trisuli, Seti, Kali Gandaki and Narayani (Fig. 1) are similar in that they all show major peaks at around ~ 2400 – 2500 Ma, which are likely to represent a combination of the Formation I and Lesser Himalayan peaks of this age. Additionally, they all contain the major Lesser Himalayan peak at ~ 1800 Ma, although this peak is especially prominent in the Trisuli and Kali Gandaki samples, perhaps because of their extended drainage networks in the Lesser Himalaya (Table 5). The Trisuli and Marsyandi distributions are somewhat unique in that the distinct peaks and deep troughs < 1000 Ma visible in the other three samples are replaced by a consistent plateau of ages.

Concentration estimates

Several trends emerge from our estimates of zircon concentration in bedrock and river sediments (Tables 2 and 3). First, our concentration estimation technique appears reliable as demonstrated by the consistent results for estimates from different aliquots of the same sample (Tables 2 and 3; column 13). Second, our results show that the concentration of zircon is widely variable in meta-sedimentary rocks as demonstrated by the differences in concentration between different bedrock samples of the same formation (Table 2; column 12). Such differences are not surprising given the tendency of zircon to become concentrated into placer deposits (Rittenhouse, 1943; Slingerland, 1977). Much greater consistency exists between samples of river sand derived from the same formation. For example, estimates of zircon concentration in Lesser Himalayan river sands show ~ 2.4 – 4.0 times higher concentrations than Greater Himalayan sands (Table 3; rows LHS-1(I) and LHS-2(H)). Although the concentrations are not directly comparable, similar relative concentrations were estimated by Amidon *et al.* (2005), who showed that Formation I has between ~ 2.2 and ~ 4.9 times higher zircon concentrations than the Lesser Himalayan rocks (Table 3).

Based on our repeated analysis of two separate sand samples from Nar Khola (Fig. 4; Table 3), one key to obtaining reliable concentration estimates from river sediments is maintaining a consistent grain size distribution between sand samples. Initially, analysis of a fine-grained sample yielded a concentration of > 50 grains g^{-1} and an average grain size about half that of other samples (Table 1; 'TSS-unused'). Analysis of a coarse-grained sample from the same site yielded a concentration of ~ 4 grains g^{-1} and an average zircon size comparable with other samples. This 10-fold, grain-size-dependent difference in zircon concentrations demonstrates the necessity

Table 5. Lithologic exposure area and average hillslope angle for individual lithologies in three Himalayan drainages

	Tethyan series			Formation II/III			Formation I			Lesser Himalaya			Miocene Granite			Unmapped			Total (km^2)
	km^2	%	Avg. slope	km^2	%	Avg. slope	km^2	%	Avg. slope	km^2	%	Avg. slope	km^2	%	Avg. slope	km^2	%	Avg. slope	
Trisuli	1474	13.1	33	N/A	N/A	N/A	3766	33.4	34.7	3403	30.1	29.8	479	4.2	37.7	2170	19.2	25.2	11 292
Seti	243	8.4	36.1	112	3.9	34.4	336	11.6	33.4	2197	76.1	23.7	N/A	N/A	N/A	N/A	N/A	N/A	2888
Kali G.	3408	29.2	27.6	161	1.4	34.7	808	6.9	32	7105	60.9	28.5	179	1.5	27.5	N/A	N/A	N/A	11 661

Avg., average.

of sampling a consistent grain size to ensure that measured concentrations are comparable.

In our predictive model, we take an area-weighted average of the two sediment concentration estimates for the Tethyan Series the single estimated sediment concentration for Formations II/III and for Formation I, and choose the higher estimate of zircon concentration given by sample LHS-1(I) to define the Lesser Himalayan concentration. The importance of choosing the higher Lesser Himalayan concentration becomes apparent during comparison of predicted and observed mixing ratios later in this paper. If the relative concentration of Formation II/III is assigned a value of 1, then our data predict that the other source areas would have relative concentrations of 3.2 for the Lesser Himalaya, 5.7 for the Tethyan Series, and 8.1 for Formation I. In calculations using main stem Marsyandi samples as one of the component PDFs, the concentration of zircon for the sample was estimated using an area-weighted average of the concentrations of upstream formations. Our zircon concentration data are in very rough agreement with unpublished data from samples collected by Christian France-Lanord from various drainages in Nepal that yielded the following zircon concentrations in bulk sediment by weight percent: Formation I: 0.57% Formation II/III: 0.22% Tethyan Series: 0.21–0.87% and Lesser Himalaya: 0.06–0.27% (E. Garzanti, Personal Communication). When our concentrations are translated to weight % the values are as follows: Formation I: 0.45–0.48%, Formation II/III: 0.07%, Tethyan Series: 0.36% and Lesser Himalaya: 0.13–0.16%. The strongest disagreement in these numbers is in the Formation II/III concentration, which will be important later in the paper.

Predicted vs. observed zircon mixing in the Marsyandi

The tabulated results of our predictive model and observed zircon mixing proportions (Fig. 7) allow an assessment of the role of different variables (exposure area, zircon concentration and erosion rates) on shaping the detrital zircon population. In Fig. 7, each column represents a different calculation of zircon mixing proportions at one of four sample sites in the Marsyandi drainage. Sample sites G and K have multiple columns because different combinations of upstream samples were used to make different mixing calculations at those sites. For example, at site K, each potential source area (Tethyan, Manaslu Granite, Formations I and II/III and Lesser Himalaya) is initially treated separately in calculation K1, whereas their contributions are amalgamated and represented by sample G in calculation K2. Formation I is also included as an independent mixing component in calculation K2 to represent Formation I sediments joining the Marsyandi below sample site G. The third possible mixing calculation (K3) uses sample E to represent the combined contribution of the Tethyan, Manaslu Granite and Formation II/III. Multiple calculations from the same site allow assess-

ment of the robustness of the predictive model and the actual mixing calculations.

One way to gauge the quality of the mixing calculation is to compare the artificial PDF created by mixing the component PDFs in their respective proportions with the observed mixed PDF (Fig. 8). The fact that the artificial and observed PDFs are well matched in all cases provides visual confirmation that reliable mixing estimates have been obtained. Because none of the Marsyandi PDFs contain ages between ~19 and 24 Ma (i.e. Deniel *et al.*, 1987; Copeland *et al.*, 1990; Harrison *et al.*, 1999), and bulk rock separations show very low zircon concentrations in the granite, we estimate the proportion of zircons derived from this source as zero in every sample and do not include this potential source in our mixing calculations.

Area prediction

To test the idea that detrital zircon populations contain zircons derived from each unit in proportion to its exposed area, we compare the exposure area predictions with the observed mixing proportions (Rows A vs. C, Fig. 7). Whereas in some cases the match between predicted and observed seems reasonable (e.g. K1, K2, G1), several obvious problems exist in the area predictions. First, calculations E, G1 and K1 show that zircons derived from the Manaslu Granite should constitute up to 6–12% of the population, yet no zircons of this age (19–24 Ma) appear in the sample. Because erosion rates are unlikely to be significantly different between Formation II/III and the Manaslu Granite, this discrepancy is likely explained by low concentrations of zircon in the granite relative to the meta-sedimentary country rocks (Table 2). This result suggests that low heavy mineral concentrations in bedrock can cause an entire region of the landscape to be underrepresented in the detrital mineral population.

A second problem with the area predictions is that every calculation treating Formation II/III individually (E, G1, K1: Fig. 7) underestimates the observed proportion of zircons from that unit (as calculated from our mixing model: row C, Fig. 7) by more than five-fold, implying that either exposure area or zircon concentration has been underestimated for this unit. The fact that similar discrepancies do


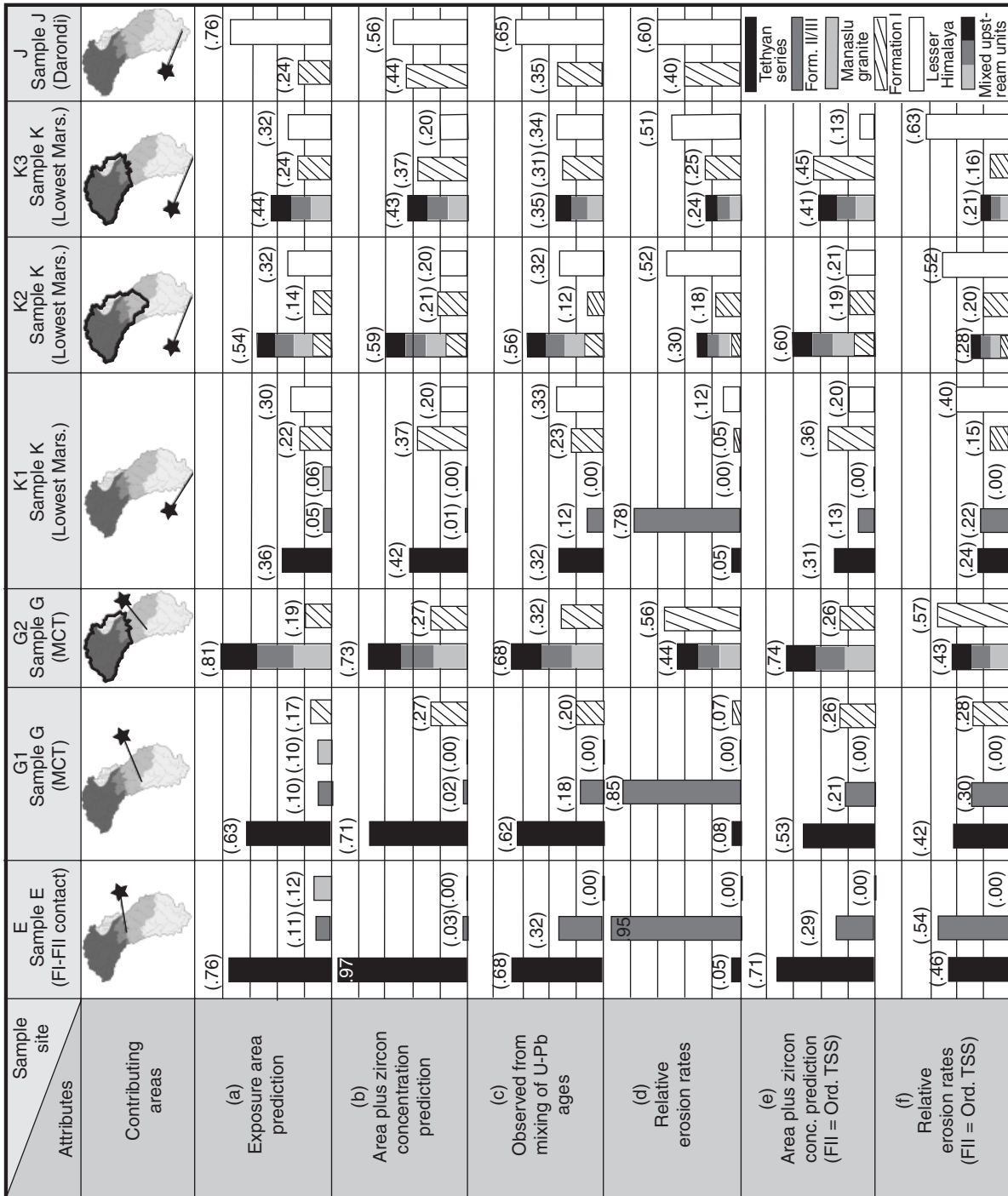


Fig. 7. This figure compares the predicted and observed mixing proportions for each of the main stem Marsyandi sample sites. A key to the colour-coding scheme is located in the lower right-hand corner. Although only four sample sites exist, multiple calculations can be made for a single site by using an upstream main stem sample to define the combined contribution of all upstream units. Rows A and B display the area-based zircon mixing prediction, and the combined area—concentration, respectively (see Fig. 6). Row C displays the observed mixing proportions at each sample site. Row D displays the modelled relative erosion rates that account for the discrepancies between rows B and C. Rows E and F show the combined prediction and modelled erosion rates, respectively, assuming that Formation II correlates with the Cambro-Ordovician Tethyan units and has a concentration of ~3.1 grains g^{-1} (see Fig. 9).



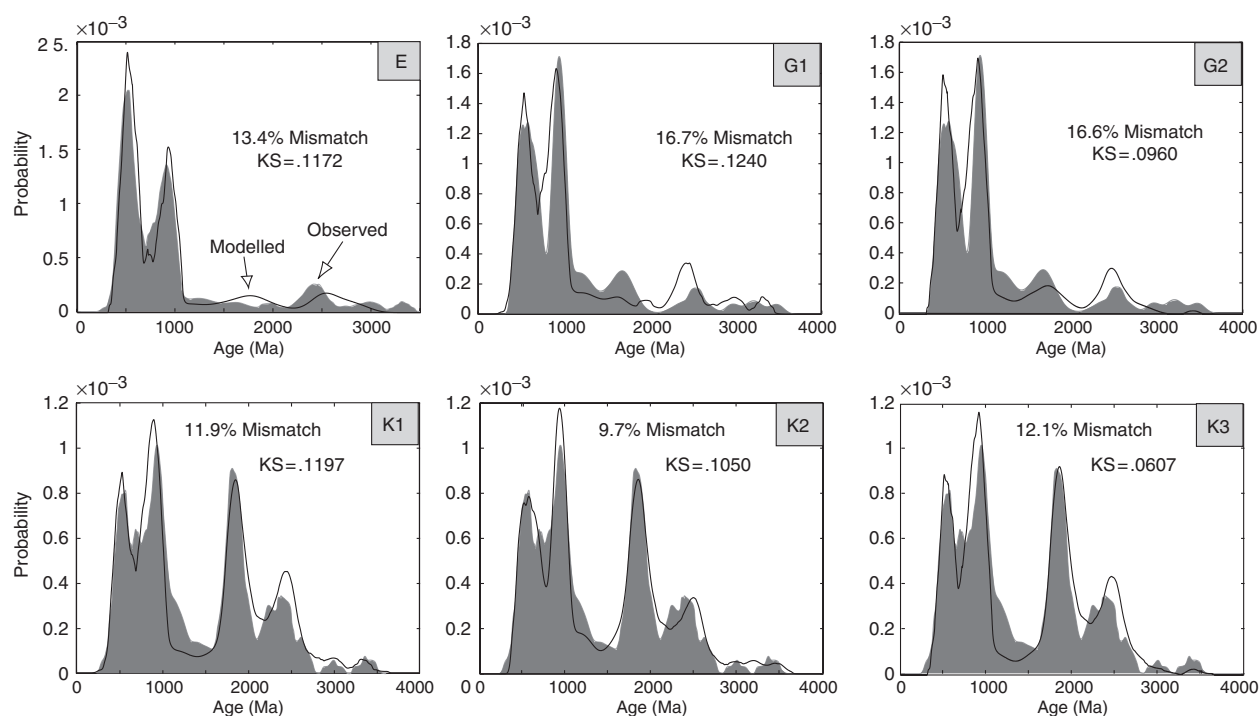


Fig 8. This figure shows the observed probability density functions (PDFs) from sample sites E, G and K (solid grey), overlain by the artificial mixed PDFs (black lines) created by combining each component PDF in the calculated proportions (Fig. 7; row C). The purpose of this figure is to demonstrate how well the ‘best match’ zircon mixing proportions calculated by the two statistical techniques actually combine to create a match with the observed PDF. The quality of the match is assessed by both percent areal mismatch (Eqn. (3)) and the Kolmogorov–Smirnov (KS) statistic. A KS statistic of > 0.1923 is required to prove any two distributions ($n = \sim 100$) are different with 95% certainty ($P = 0.05$).

not occur in calculations using samples E and K (columns G2, K3; Fig. 7) from the main stem supports this explanation by showing that the underestimate is specific to Formation II/III and does not occur when considering all lithologies above the Formation I–II contact as a whole. Later in the paper, we will attribute this, in part, to an underestimate of the Formation II/III exposure area.

Combined area–concentration predictions and modelled erosion rates

The eight-fold differences in zircon concentrations (Table 3) dictate that, when formational exposure areas are combined with zircon concentrations specific to each formation, the predicted contributions for given formations should change several fold in comparison with that based on area alone (rows A, B; Fig. 7). Instead of improving the prediction, applying a correction for the concentration of zircon in each contributing unit seems to worsen the prediction in almost every case (Fig. 7). Given that we expect neither attrition of zircon nor a systematic sampling bias to affect the observed age distributions, another explanation must be sought. One obvious possibility is that the relative zircon concentrations we use are incorrect. To define concentrations of zircon in river sediments with a high degree of accuracy would require many samples from each contributing drainage. However, our ability to duplicate concentration estimates among samples

(Tables 2 and 3) and our rough agreement with the independent data above suggest that the overall trends in concentration estimates are valid. Acknowledging this assumption, we speculatively attribute the poorer predictions that result from including zircon concentration (rows B and C, Fig. 7) to the happenstance of an inverse relationship between zircon concentration and relative erosion rate in the upper and lower part of the drainage: higher erosion rates in the Lesser Himalaya may offset its lower zircon concentration (see ‘Discussion’). Similarly, high zircon concentrations in the Tethyan Series and Formation I offset their lower erosion rates. The result of these counterbalances is a relatively equal zircon flux per unit area from all units. Thus, the match between the observed and predicted mixing proportions evolves from a fairly good approximation using just area, becomes worse after factoring in concentration and returns to a good match once fitted erosion rates (row D, Fig. 7) are factored in. Assuming relative zircon concentrations are approximately correct, erosion rates need to be ~ 2 times higher in the Lesser Himalaya than in the Tethyan Series and Formation I to account for observed zircon mixing. Although this is a surprising result, had we chosen to use the lower zircon concentration estimate for the Lesser Himalaya (Table 3; LHS-2), predicted erosion rates would have appeared to be even higher in this unit. Interestingly, erosion rates would need to be roughly balanced between the Tethyan Series and Formation I to satisfy the observed data.

Proposed correlation of Formation II and the lower Tethyan Series

Unrealistically high modelled erosion rates for Formation II/III (row D, Fig. 7) result from the fact that Formation II/III contributed higher proportions of zircon than predicted by the area–concentration predictions. One likely explanation for this discrepancy is that Formation II is the high-grade metamorphic equivalent of some of the Cambro–Ordovician Tethyan Series units, such as the Annapurna Yellow and Nilgiri Formations (Fig. 2) (Le Fort, 1975). If this is true, then these units would also be expected to contribute a ‘Formation II/III’ age distribution, thus increasing the source area for such ages by >three-

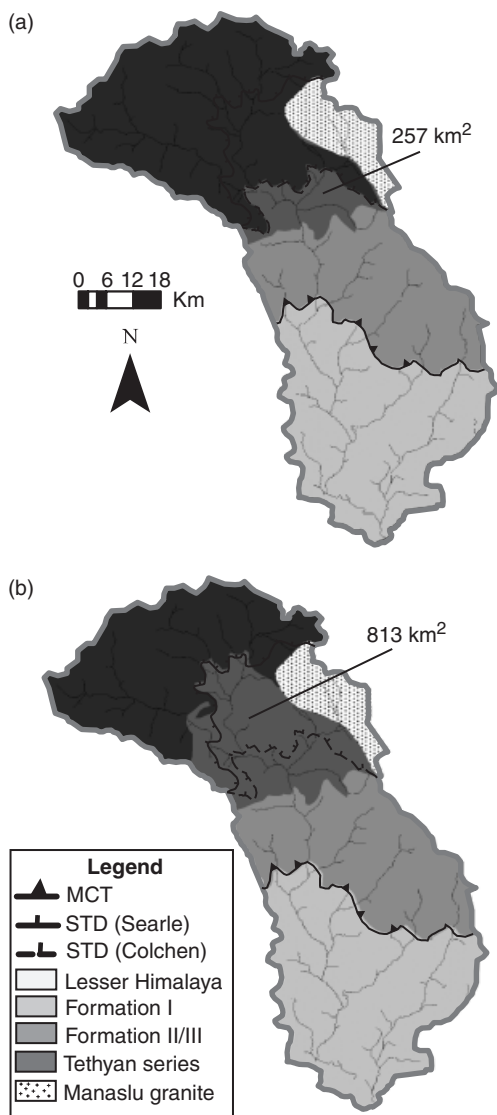


Fig. 9. Panel A shows the Marsyandi drainage as mapped by Colchen *et al.* (1986) and Searle & Godin (2003) in which Formation II comprises an area of ~ 257 km². Panel B shows the Marsyandi drainage assuming that Formation II is correlative with the Cambro–Ordovician Tethyan units as proposed by Le Fort (1975). In this scenario, the source area for ‘Formation II/III’ zircon ages increases to ~ 813 km².

fold from ~ 257 to ~ 813 km² (Fig. 9). This idea fits well with the model of Gehrels *et al.* (2003), who proposed that uplift and erosion of Greater Himalayan rocks in the Mid–Ordovician marked a shift in the depositional regime of the Indian margin. This implies that Formation II and the Cambro–Ordovician Tethyan units received detrital zircons from the same source until the Mid–Ordovician and should thus share the same age distribution. To evaluate the viability of this explanation, we recalculated the predicted mixing proportions using the larger exposure area. Interestingly, the larger source area for Formation II/III zircons still predicts lower proportions of Formation II/III zircon ages than are observed (row E, Fig. 7). This result suggests that we may also have underestimated the concentration of zircon contributed from Formation II/III by measuring it in river sediments draining predominantly carbonate units, when the expanded source area for Formation II/III ages includes more pelitic and siliciclastic strata. We found that a Formation II/III concentration ~ 4 times higher than originally estimated gave the best match to observed mixing results. This explanation is supported by comparison of our data with the unpublished data presented in the ‘Concentration Estimates’ section, where our estimate of Formation II/III concentration is ~ 3 times lower than that of France–Lanord.

Comparison of adjacent drainages

The second part of our study compares U–Pb age distributions from four adjacent drainage basins spanning ~ 250 km along the axis of the Nepal Himalaya, and from a fifth sample taken below their confluence (Fig. 1). The purpose of this comparison is to evaluate the spatial homogeneity of the detrital U–Pb zircon age distribution on the orogen scale and determine the causes of spatial variability. To quantify differences between the distributions, we compared cumulative frequency distributions (Fig. 10) and the KS statistic (Table 6) between samples. None of the sample pairs exceeds the critical KS statistic for $P = 0.1$ (Table 6); they are thus statistically indistinguishable. However, given that the KS statistic itself is a measure of similarity between two distributions, the lowest values indicate the detrital populations that are most similar (Table 6). Across central Nepal, the western drainages (Seti and Kali Gandaki) are the most similar, whereas the Trisuli does not yield a low KS statistic with any drainages suggesting slight east–west differences in the detrital ages.

The Trisuli age distribution is visually unique because it has a plateau of age probability between ~ 500 and 1000 Ma where other distributions have two distinct peaks near ~ 500 and ~ 1000 Ma. This difference may be explained by a larger proportion of Formation I zircon ages in the Trisuli age distribution, which have a more evenly distributed age probability between 500 and 1000 Ma (panel A, sample ‘F’ and panel C; Fig. 3), whereas the Tethyan Series and Formation II/III distributions are characterized by large peaks at between 500 – 600 and 900 – 1000 Ma

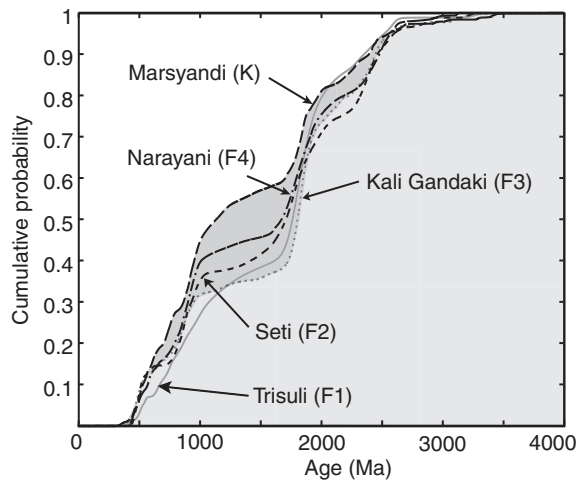


Fig. 10. Cumulative probability distributions for the Trisuli, Marsyandi, Seti, Kali Gandaki and Narayani rivers. The cumulative probability at any given age represents the total area under the sample probability density function younger than the given age.

Table 6. KS statistics from comparison of U–Pb zircon age distributions between drainages

		Trisuli (F1)	Marsyandi (K)	Seti (F2)	Kali G. (F3)
	<i>n</i>	<i>n</i> = 96	<i>n</i> = 217	<i>n</i> = 99	<i>n</i> = 101
Narayani (F4)	174	0.092	0.1208	0.0543	0.067
Kali G. (F3)	101	0.134	0.1225	0.0823	
Seti (F2)	99	0.108	0.0867		
Marsyandi (K)	217	0.115			

KS, Kolmogorov–Smirnov.

(panels B and C, Fig. 3; Fig. 4). This explanation fits with the observation that the exposure area of Formation I increases significantly to the east, whereas exposure area of Formation II decreases to the east (Le Fort, 1975; Colchen *et al.*, 1986). However, because of the use of a 1 : 500 000 scale map, Fig. 1 does not accurately depict this trend. This interpretation is further supported by the fact that the observed ratio of zircons derived from FII : FI changes from $\sim 1 : 4$ in the Trisuli to $\sim 2 : 3$ in the Kali Gandaki (Fig. 11).

Mixing calculations to determine the proportion of zircons derived from each unit were compared with area-concentration predictions for the four adjacent drainages (Fig. 11). The accuracy of these predictions is again dependent upon concentration estimates made from the limited sample set in Table 3 and extrapolated across large drainage areas (Amidon *et al.*, 2005). Assuming the concentration estimates are roughly correct, the observed proportion of Lesser Himalayan zircons in most drainages is higher than predicted based on area and concentration. This agrees with our previous interpretation that higher erosion rates in the Lesser Himalaya compensate for its lower zircon concentration.

A second observation is that the over-representation of Formation II/III increases in magnitude from east to west. This may reflect the fact that the exposure area of Formation II tapers to the east. Alternatively, it may reflect the fact that the Tethyan Series in the Kali Gandaki is largely Cambro–Ordovician in age (thus providing ‘Formation II/III’ zircon ages), while it is largely post-Ordovician in the Trisuli drainage. Likewise, in Seti Khola, the over-representation of Formation II/III zircons could be explained by the fact that it contains only pre-Ordovician Tethyan units. A third observation is that the Tethyan Series is under-represented in both the Kali Gandaki and Trisuli. This probably reflects the fact that the Tethyan Series is exposed in the upper reaches of these drainages on the southernmost Tibetan Plateau where arid conditions and low relief promote lower erosion rates.

The Narayani sample (Sample F4, Figs 2 and 12) integrates contributions from all four catchments and does not seem to be dominated by any one of them, nor by any single unit. Based on visual inspection and comparison of KS statistics, the Narayani sample is not statistically different from any of the four contributing samples (Table 6). Observed zircon mixing proportions in the Narayani sample (Fig. 11) suggest that it contains zircons derived from each of the major upstream formations.

DISCUSSION

The advent of low-cost, high-precision and rapid U–Pb dating of zircon has ushered in an era whereby hundreds of grains can be dated in a single study. With sufficient numbers of grains, the age distribution of various source areas can be reliably characterized. Such characterizations provide a practical means to address several key questions, ranging from the geometry of ancient continents to the evolution of the detrital zircon signal as it passes through various source areas within an orogen. We have focused on this latter question in the central Himalaya, where we have dated more than 2400 zircons from 21 samples. These ages provide a robust characterization of the age distributions in their source areas and reveal striking downstream changes in the detrital zircon population of a major Himalayan river system. In addition, when two well-characterized populations of ages from different source areas mix downstream to produce a third population, the relative contribution from each source can be readily calculated through iterative or inverse modelling, and mixing calculations for successive populations can illuminate the evolution of the downstream age signal as a specific mixture of upstream sources.

In many studies in which detrital minerals are used for geochronology, lithologically or spatially dependent differences in the concentration of the minerals being measured are commonly undocumented. Using a new approach to estimate zircon concentrations (Amidon *et al.*, 2005), we show here in the Marsyandi catchment of central Himalaya that zircon concentrations in bedrock vary by at least

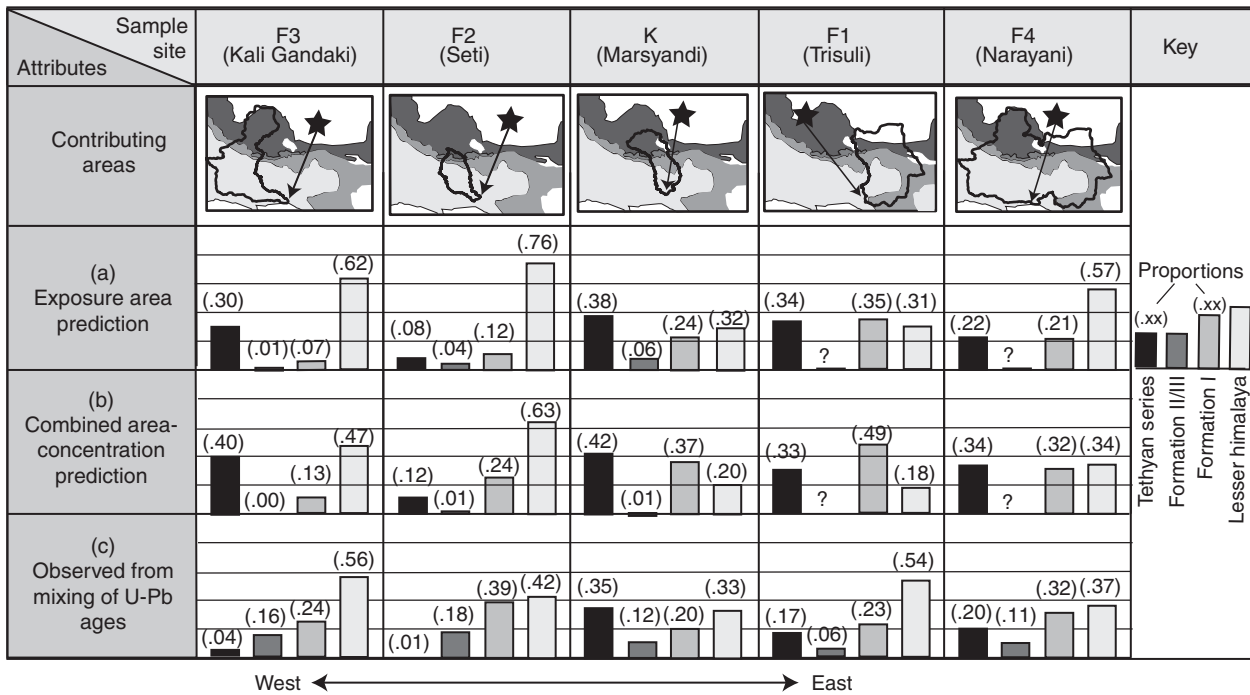


Fig. 11. This figure displays the predicted and observed mixing proportions for the Trisuli, Marsyandi, Seti, Kali Gandaki and Narayani samples. Each column represents the calculation made for a given drainage. Rows A and B display the lithologic exposure area prediction and the combined area–concentration prediction, respectively. All unmapped regions of the Trisuli are assigned to the Tethyan Series in this prediction. Question marks indicate that the proportion of Formation II/III is unknown and was not included in the prediction. Row C displays the observed mixing proportions.

18-fold within the same formation and can show strong spatial variation, particularly in sedimentary and meta-sedimentary rocks. In contrast, small catchments draining single geologic units yield spatially averaged results that provide a more reliable estimate of zircon concentration in a given formation. In the central Himalaya, such estimates indicate eight-fold differences in detrital zircon concentrations among four major geologic units. Within this same catchment, detrital muscovite concentrations are estimated to vary by up to 100-fold (2003). These two studies suggest that variations in mineral concentrations should be further investigated. Moreover, this study suggests that a similar grain size should be analysed in all samples. For example, we found more than 10-fold differences in zircon concentrations between coarse and medium sand-sized samples from the same site. We have not developed an automated or rapid means to estimate the zircon concentration, but we have shown that the product of the mean zircon grain size and its concentration scales with the Zr concentration (Amidon *et al.*, 2005).

The contribution from any region of the landscape to the zircon signal in the trunk stream should scale with its exposure area, zircon concentration and erosion rate. In this study, as much as 12% of some catchments contain zircon-poor rocks, such that they are completely undetectable in the detrital signal. In large catchments, where it may be impractical to characterize all major source units, uncertainties result from generalizing from specific sites to broader areas. For example, in the present study we treat

Table 7. Critical KS statistics for a given combination of sample sizes and *P*-values

<i>P</i> -value	Paired sample sizes			
	100 vs. 100	100 vs. 174	100 vs. 217	174 vs. 217
0.01	0.2305	0.2045	0.1970	0.1659
0.05	0.1923	0.1707	0.1644	0.1384
0.1	0.1725	0.1531	0.1475	0.1241
0.2	0.1513	0.1343	0.1293	0.1089

KS, Kolmogorov–Smirnov. Sheskin, 2003.

the Tethyan Series as a single unit, even though it comprises carbonates and siliclastics that have highly contrasting zircon concentrations. We define the zircon age distributions based on two samples from catchments within the Tethyan rocks (Fig. 4). We did not specifically sample Cambro–Ordovician Tethyan strata, and yet we now suspect that they contain an age signal that is more equivalent to that of Formation II than to that of the ‘Tethyan’ population that we defined.

When we assume this equivalency in our calculations, we reduce the relative erosion rate of Formation II/III by 40–80% (row D vs. F: Fig. 7). Without such an assumption, the erosion rates for Formation II/III are calculated to be 5–10 times higher than that of any other lithologic unit. We know of no observations or deformational/erosional mechanisms that would support such a high rate across a narrow swath along the Greater Himalaya. We are forced

to conclude that either our age characterization or estimates of zircon concentrations of Formation II/III are incorrect, or that a larger area with equivalent age populations is contributing to the detrital signal, or both.

Both within the Marsyandi catchment and across the four studied large catchments, our calculations predict that the Lesser Himalaya is eroding faster than the Greater Himalaya (Figs 8 and 12). Although we acknowledge the likelihood of large errors in our estimation of zircon concentrations, our calculations use the highest zircon concentration measured in the Lesser Himalaya (Table 3), which should minimize its modelled erosion rate. Given that modelled Lesser Himalayan erosion rates should be conservative, the consistently higher rates may reflect actual variations in erosion rate. This hypothesis is not unreasonable in light of other data from central Nepal. First, topographic and structural indicators as well as young detrital muscovite $^{40}\text{Ar}/^{39}\text{Ar}$ ages suggest MCT footwall deformation has persisted to the present (Wobus *et al.*, 2003; Hodges *et al.*, 2004). Second, monsoon precipitation is higher in the Lesser Himalaya than it is in the Greater Himalaya and Tethyan rocks. Most of the Lesser Himalaya in the Marsyandi region receives $\sim 2 \text{ m yr}^{-1}$ of monsoonal rain. This rainfall reaches a maximum ($3.5 - 4.5 \text{ m yr}^{-1}$) near the boundary between the Lesser and Greater Himalaya, decreases to $< 2 \text{ m yr}^{-1}$ above Formations I–III and drops to as low as 0.4 m yr^{-1} above the northern outcrops of the Tethyan Series (Barros *et al.*, 2000; Gabet *et al.*, 2004). If erosion rate and precipitation are correlative, as has been suggested in other orogens, we might expect higher erosion rates in the Lesser Himalaya than in other regions (Fuller *et al.*, 2003; Reiners *et al.*, 2003). Third, our previous results show clear evidence for approximately three-fold higher erosion rates in the footwall of the traditional MCT based on mixing of U–Pb zircon ages in two drainages (Amidon *et al.*, 2005).

The evidence supporting rapid Lesser Himalayan erosion is, however, not unequivocal and there are several lines of conflicting evidence. Vance *et al.* (2003) used cosmogenic isotope inventories to show that erosion rates were ~ 2 times faster in the Higher Himalaya than in the adjacent foothills, $\sim 500 \text{ km}$ west of our field area. Apatite fission-track data indicate significantly more rapid erosion across the Greater Himalaya (Burbank *et al.*, 2003). Mean elevations and relief are higher, hillslopes are steeper in the Greater Himalaya (Gabet *et al.*, 2004) and Pleistocene glaciers, with their great erosive capacities (Hallet *et al.*, 1996), are almost exclusively found within the Greater Himalaya and Tethyan realms.

Finally, even reliable studies of relative erosion rates using modern detrital sediments provide only a snapshot in time. The extent to which the present interglaciation is representative of average long-term rates is unknown, as is the extent to which today's detrital minerals are representative of the Holocene. Within the Holocene, for example, the Marsyandi appears to have gone from being under capacity with respect to its sediment load to over capacity and back again (Pratt *et al.*, 2002).

CONCLUSIONS

We use mixing of U–Pb zircon age distributions in modern river sediments to test the assumption that the detrital mineral population provides a representative sample of the upstream drainage area. Specifically, we explore the importance of three variables, lithologic exposure area, bedrock zircon concentration and differential erosion rates, in shaping the detrital mineral population. First, we show that zircon concentrations in bedrock samples from the same unit vary by up to 18-fold, whereas estimating concentrations of zircon in river sediments draining a single unit provides a more accurate method with which to define the average zircon concentration of a given unit.

Combining these concentration estimates with the relative exposure area of each unit in the Marsyandi drainage, we predict the proportion of zircon that should be derived from each lithology and compare it with observed mixing proportions. A key result is that the Manaslu granite constitutes up to 12% of the drainage area upstream of some samples, but contributes no measured zircon ages because of its relatively low zircon concentration. In contrast, Formations II and III contribute more zircons than expected. In light of the proposed correlation of Formation II with lower Tethyan units, we explain this discrepancy by suggesting that the actual area from which these ages are derived in the Marsyandi catchment is ~ 3 times larger than expected, and zircon concentrations are higher than measured. Comparisons between predicted and observed zircon mixing proportions for all units reveal that erosion rates may be, on average, twice as high in the Lesser Himalaya to account for the observed discrepancy between predicted and observed mixing proportions.

Comparison of samples from four adjacent drainages spanning $\sim 250 \text{ km}$ along the Himalayan front reveals that their U–Pb zircon age distributions are not statistically different. However, based on visual observation and comparison of KS statistics, slight differences exist in the age distributions from east to west. These differences may be attributable to different exposure areas of Formations I and II along the Himalayan front and lower erosion rates along the southern Tibetan Plateau.

Overall, we found that numerical mixing and unmixing of U–Pb ages is an appropriate way to fingerprint zircon populations and trace them through an orogen from bedrock to foreland sediment. Inherent difficulties in correlating units, quantifying zircon concentrations and assigning erosion rates to specific units limit the accuracy of our predictive model. Despite significant uncertainties, we clearly demonstrate the potential for detrital mineral populations to be biased by variable zircon concentrations and differential erosion rates in the source region. We also apply new methods for establishing lithologic exposure area and relative zircon concentrations that could be used in any detrital study to make general predictions about the source areas for various detrital mineral suites. This technique could also be coupled with heavy-mineral point counting (i.e. Morton, 1991; Garzanti *et al.*, 2004; Garzanti

et al., 2005), Gaussian peak fitting (i.e. Brandon, 1992; Sambridge & Compston, 1994), double dating by U–Pb and U–Th/He (Rahl *et al.*, 2003) or mixing of other geochemical characteristics (i.e. Hoskin & Ireland, 2000) to further refine the accuracy of mixing estimates.

ACKNOWLEDGEMENTS

We thank Luc Mehl, Nathan Niemi, Gabriel Rotberg, Michael Oskin, Beth Pratt-Sitaula and the Hacker Lab for their insight and assistance. We thank Peter DeCelles, Eduardo Garzanti and Matthias Bernet for thorough and thoughtful reviews, which greatly improved this manuscript. Support for this research was received from NSF Continental Dynamics [EAR 9909647]. Logistical arrangements were provided by Himalayan Experience.

REFERENCES

- AMIDON, W.H., BURBANK, D.W. & GEHRELS, G.E. (2005) U–Pb zircon ages as a sediment mixing tracer in the Nepal Himalaya. *Earth Planet. Sci. Lett.*, **235**, 244–260.
- BARROS, A., JOSHI, M., PUTKONEN, J. & BURBANK, D.W. (2000) A study of the 1999 monsoon rainfall in a mountainous region of central Nepal using TRMM products and rain gauge observations. *Geophys. Res. Lett.*, **27**, 3683–3686.
- BEHERA, P. (2003) Heavy minerals in beach sands of Gopalpur and Paradeep along the Orissa coastline, east coast of India. *Indian J. Mar. Sci.*, **32**, 172–174.
- BERNET, M., BRANDON, M.T., GARVER, J.I. & MOLITER, B. (2004) Fundamentals of zircon fission-track analysis for provenance and exhumation studies with examples from the European Alps. *Geol. Soc. Am. Spec. Paper*, **378**, 25–36.
- BERRY, R.F., JENNER, G.A., MEFFRE, S. & TUBRETT, M.N. (2001) A North American provenance for Neoproterozoic to Cambrian sandstones in Tasmania? *Earth Planet. Sci. Lett.*, **56**, 336–342.
- BRANDON, M.T. (1992) Decomposition of fission-track grain-age distributions. *Am. J. Sci.*, **292**, 535–564.
- BREWER, I.D., BURBANK, D.W. & HODGES, K.V. (2003) Modelling detrital cooling-age populations; insights from two Himalayan catchments. *Basin Res.*, **15**, 305–320.
- BURBANK, D.W., BLYTHE, A.E., PUTKONEN, J., PRATT-SITaula, B., GABET, E., OSKIN, M., BARROS, A. & OJHA, T.P. (2003) Decoupling of erosion and precipitation in the Himalaya. *Nature*, **426**, 652–655.
- COLCHEN, M., LE FORT, P. & PECHER, A. (1986) *Geological Researches in the Nepal Himalaya, Annapurna–Manaslu–Ganesh Himal; Notice of the Geological Map on 1/200 000*, 1st edn. Centre National de la Recherche Scientifique, Paris.
- COLEMAN, M.E. (1996) Orogen-parallel and orogen-perpendicular extension in the central Nepalese Himalayas. *Geol. Soc. Am. Bull.*, **108**, 1594–1607.
- COPELAND, P., HARRISON, M. & LE FORT, P. (1990) Age and cooling history of the Manaslu granite: implications for Himalayan tectonics. *J. Volcanol. Geotherm. Res.*, **44**, 33–50.
- CULLERS, R.L. & GRAF, J.L. (1984) Rare earth elements in igneous rocks of the continental crust: Intermediate and silicic rocks. In: *Rare Earth Element Geochemistry*, 1st edn (Ed. by P. Henderson), pp. 275–308. Elsevier, Amsterdam.
- DADSON, S.J., HOVIUS, N., CHEN, H., DADE, W.B., HSIEH, M.L., WILLETT, S.D., HU, J.C., HORNG, M.J., CHEN, M.C., STARK, C.P., LAGUE, D. & LIN, J.C. (2003) Links between erosion, runoff variability and seismicity in the Taiwan orogen. *Nature*, **426**, 648–651.
- DAY, S.J. & FLETCHER, W.K. (1991) Concentration of magnetite and gold at bar and reach scales in a gravel-bed stream, British Columbia, Canada. *J. Sediment. Petrol.*, **61**, 871–882.
- DECELLES, P.G., GEHRELS, G.E., NAJMAN, Y., MARTIN, A.J., CARTER, A. & GARZANTI, E. (2004) Detrital geochronology and geochemistry of cretaceous-early miocene strata of Nepal: implications for timing and diachroneity of initial Himalayan orogenesis. *Earth Planet. Sci. Lett.*, **227**, 313–330.
- DECELLES, P.G., GEHRELS, G.E., QUADE, J., LAREAU, B. & SPURLIN, M. (2000) Tectonic implications of U–Pb Zircon ages of the Himalayan orogenic belt in Nepal. *Science*, **288**, 497–499.
- DECELLES, P.G., GEHRELS, G.E., QUADE, J., OJHA, T.P., KAPP, P.A. & UPRETI, B.N. (1998) Neogene foreland basin deposits, erosional unroofing, and the kinematic history of the Himalayan fold-thrust belt, western Nepal. *Geol. Soc. Am. Bull.*, **110**, 2–21.
- DECELLES, P.G., ROBINSON, D.M., QUADE, J., OJHA, T.P., GARZIONE, C.N., COPELAND, P. & UPRETI, B.N. (2001) Stratigraphy, structure and tectonic evolution of the Himalayan fold and thrust belt in western Nepal. *Tectonics*, **20**, 487–509.
- DEGRAAF-SURPLESS, K., MAHONEY, J.B., WOODEN, J.L. & MCWILLIAMS, M.O. (2003) Lithofacies control in detrital zircon provenance studies: insights from the cretaceous methow basin, southern Canadian Cordillera. *Geol. Soc. Am. Bull.*, **115**, 899–915.
- DENIEL, C., VIDAL, P., FERNANDEZ, A., LE FORT, P. & PEUCAT, J.J. (1987) Isotopic study of the manaslu granite (Himalaya, Nepal): inferences on the age and source of Himalayan leucogranites. *Contrib. Mineral. Petrol.*, **96**, 78–92.
- DICKINSON, W.R. & GEHRELS, G.E. (2003) U–Pb ages of detrital zircons from Permian and Jurassic eolian sandstones of the Colorado Plateau, USA: paleogeographic implications. *Sediment. Geol.*, **163**, 29–66.
- EHLERS, T.A. & FARLEY, K.A. (2003) Apatite (U–Th)/He thermochronometry: methods and applications to problems in tectonic and surface processes. *Earth Planet. Sci. Lett.*, **206**, 1–14.
- FREY, F.A. (1984) Rare earth elements abundances in upper mantle rocks. In: *Rare Earth Element Geochemistry*, 1st edn (Ed. by P. Henderson), pp. 82–106. Elsevier, Amsterdam.
- FRIHY, O.E., LOFTY, M.F. & KOMAR, P.D. (1995) Spatial variations in heavy minerals and patterns of sediment sorting along the Nile Delta, Egypt. *Sediment. Geol.*, **97**, 33–41.
- FUCHS, G.R. (1980) *The Lesser Himalayan Geology of West Nepal and its Regional Importance*, 1st edn. Hindustan Publishing Corporation, Delhi.
- FULLER, C.W., WILLETT, S.D., HOVIUS, N. & SLINGERLAND, R. (2003) Erosion rates for Taiwan mountain basins; new determinations from suspended sediment records and a stochastic model of their temporal variation. *J. Geol.*, **111**, 71–87.
- GABET, E., PRATT-SITaula, B. & BURBANK, D.W. (2004) Climatic controls on hillslope angle and relief in the Himalayas. *Geology*, **32**, 629–632.
- GANSSE, A. (1964) *Geology of the Himalayas*. Wiley-Interscience, New York, 1964.
- GARVER, J.I., BRANDON, M.T., RODEN-TICE, M. & KAMP, P.J. (1999) Exhumation history of orogenic highlands determined by detrital fission-track thermochronology. In: *Exhumation*

- Processes: Normal Faulting, Ductile Flow and Erosion*, 1st edn (Ed. by U. Ring, M.T. Brandon, G.S. Lister & S.D. Willett), pp. 283–304. Geological Society, London.
- GARZANTI, E., VEZZOLI, G., ANDO, S., FRANCE-LANORD, C., SINGH, S.K. & FOSTER, G. (2005) Sand petrology and focused erosion in collision orogens: the Brahmaputra case. *Earth Planet. Sci. Lett.*, **220**, 157–174.
- GARZANTI, E., VEZZOLI, G., LOMBARDO, B., ANDO, S., MAURI, E., MONGUZZI, S. & RUSSO, M. (2004) Collision-orogen provenance (Western Alps): detrital signatures and unroofing trends. *J. Geol.*, **112**, 145–164.
- GEHRELS, G.E., DECELLES, P.G., MARTIN, A., OJHA, T.P. & PINHASSI, G. (2003) Initiation of the Himalayan orogen as an early paleozoic thin-skinned thrust belt. *Today*, **13**, 4–9.
- GRUJIC, D., HOLLISTER, L.S. & PARRISH, R.R. (2002) Himalayan metamorphic sequence as an orogenic channel: insight from Bhutan. *Earth Planet. Sci. Lett.*, **198**, 177–191.
- GROMET, L.P. & SILVER, L.T. (1983) Rare earth element distributions among minerals in a granodiorite and their petrogenetic implications. *Geochim. Cosmochim. Acta*, **47**, 925–939.
- HALLET, B., HUNTER, L. & BOGEN, J. (1996) Rates of erosion and sediment evacuation by glaciers: a review of field data and their implications. *Global Planet. Change*, **12**, 213–235.
- HARRISON, M., GROVE, M., MCKEEGAN, K.D., COATH, C.D., LOVERA, O.M. & LE FORT, P. (1999) Origin and episodic emplacement of the Manaslu intrusive complex, central Himalaya. *J. Petrol.*, **40**, 3–19.
- HODGES, K.V. (2000) Tectonics of the Himalaya and southern Tibet from two perspectives. *Geol. Soc. Am. Bull.*, **112**, 324–350.
- HODGES, K.V., PARRISH, R.R. & SEARLE, M.P. (1996) Tectonic evolution of the central Annapurna Range, Nepalese Himalayas. *Tectonics*, **15**, 1264–1291.
- HODGES, K.V., WOBUS, C., RUHL, K., SCHILDGEN, T. & WHIPPLE, K.X. (2004) Quaternary deformation, river steepening and heavy precipitation at the front of the Higher Himalayan ranges. *Earth Planet. Sci. Lett.*, **220**, 374–389.
- HOLT, D.N. (1965) The Kangankunde Hill rare earth prospect. *Bull. Geol. Survey Dept. Malawi*, **20**, 130.
- HOSKIN, P.O. & IRELAND, T.R. (2000) Rare earth element chemistry of zircon and its use as a provenance indicator. *Geology*, **28**, 627–630.
- HUBERT, J.F. (1971) Analysis of heavy mineral assemblages. In: *Procedures in Sedimentary Petrology*, 1st edn (Ed. by R.E. Carver), pp. 453–478. Wiley, New York.
- JONES, H.A. & DAVIES, P.J. (1979) Preliminary studies of offshore placer deposits, Eastern Australia. *Mar. Geol.*, **30**, 243–268.
- KARVE, V.M., MADHAVEN, T.R. & SOMNAY, J.Y. (1966) Mineral recovery from beach sands. *Mineral. Mag.*, **114**, 10–15.
- LAVÉ, J. & AVOUAC, J.P. (2000) Active folding of fluvial terraces across the Siwalik Hills, Himalayas of central Nepal. *J. Geophys. Res.*, **105**, 5735–5770.
- LE FORT, P. (1975) Himalayas; the collided range; present knowledge of the continental arc. *Am. J. Sci.*, **275A**, 1–44.
- LIHOU, J.C. & MANGE-RAJETZ, K.Y. (1996) Provenance of the Sardona Flysch, eastern Swiss Alps: example of high resolution heavy mineral analysis applied to an ultrastable assemblage. *Sediment. Geol.*, **105**, 141–157.
- MARTIN, A., DECELLES, P.G., GEHRELS, G.E., PATCHETT, P.J. & ISACHSEN, C. (2005) Isotopic and structural constraints on the location of the main central thrust in the Annapurna Range, central Nepal Himalaya. *Geol. Soc. Am. Bull.*, **117**, 926–944.
- MENKE, W. (1989) *Geophysical Data Analysis: Discrete Inverse Theory*, 2nd edn. Academic Press, San Diego.
- MORTON, A.C. (1985) Heavy minerals in provenance studies. In: *Provenance of Arenites*, 1st edn (Ed. by G.G. Zuffa), pp. 249–277. Reidel, Dordrecht.
- MORTON, A.C. (1991) Geochemical studies of detrital heavy minerals and their application to provenance research. In: *Developments in Sedimentary Provenance Studies*, edn (Ed. by A.C. Morton, S.P. Todd & P.D.W. Haughton), pp. 31–45. Royal Geological Society.
- MORTON, A.C. & HALLSWORTH, C.R. (1994) Identifying provenance-specific features of detrital heavy mineral assemblages in sandstones. *Sediment. Geol.*, **90**, 241–256.
- MORTON, A.C. & HALLSWORTH, C.R. (1999) Processes controlling the composition of heavy mineral assemblages in sandstones. *Sediment. Geol.*, **124**, 3–29.
- MORTON, A.C. & JOHNSON, M.J. (1993) Factors influencing the composition of detrital heavy mineral suite in Holocene sands of the Apure River drainage basin, Venezuela. *Geol. Soc. Am. Spec. Paper*, **284**, 171–185.
- MORTON, A.C. & SMALE, D. (1991) The effects of transport and weathering on heavy minerals from the Cascade River, New Zealand. *Sediment. Geol.*, **68**, 117–123.
- MYROW, P.M., HUGHES, N.C., PAULSEN, T.S., WILLIAMS, I.S., PARCHA, S.K., THOMPSON, K.R., BOWRING, S., PENG, S.C. & AHLUWALIA, J. (2003) Integrated tectonostratigraphic analysis of the Himalaya and implications for its tectonic reconstruction. *Earth Planet. Sci. Lett.*, **212**, 433–441.
- NEARY, C.R. & HIGHLEY, D.E. (1984) The economic importance of the rare earth elements. In: *Rare Earth Element Geochemistry*, 1st edn (Ed. by P. Henderson), pp. 247–273. Elsevier, Amsterdam.
- OVERSTREET, W.C. (1967) *The Geologic Occurrence of Monazite*, 1st edn. U.S. Geological Survey, Washington.
- PEARSON, O.N. & DECELLES, P.G. (2005) Structural geology and regional tectonic significance of the Ramgarh thrust, Himalayan fold-thrust belt of Nepal. *Tectonics*, **24**(4), TC400810.1029/2003TC001617.
- POITRASSON, F., HANCHAR, J.M. & SCHALTEGGER, U. (2002) The current state and future of accessory mineral research. *Chem. Geol.*, **19**, 3–24.
- POLDERVAART, A. (1956) Zircon in rocks. 2. Igneous rocks. *Am. J. Sci.*, **254**, 521–554.
- POWERS, P.M., LILLIE, R.J. & YEATS, R.S. (1998) Structure and shortening of the Kangra and Dehra Dun reentrant, sub-Himalaya, India. *Geol. Soc. Am. Bull.*, **110**, 1010–1027.
- PRATT, B., BURBANK, D.W., HEIMSATH, A. & OJHA, T.P. (2002) Impulsive alluviation during early Holocene strengthened monsoons, central Nepal Himalaya. *Geology*, **30**, 911–914.
- PRESS, W.H. (1997) *Numerical Recipes in C: The Art of Scientific Computing*, 2nd edn. Cambridge University Press, Cambridge.
- RAHL, J.M., REINER, S.P.W., CAMPBELL, I.H., NICOLESCU, S. & ALLEN, C.M. (2003) Combined single-grain (U–Th)/He and U/Pb dating of detrital zircons from the Navajo Sandstone, Utah. *Geology*, **31**, 761–764.
- REINERS, P.W., EHLERS, T.A., MITCHELL, S.G. & MONTGOMERY, D.R. (2003) Coupled spatial variations in precipitation and long-term erosion rates across the Washington Cascades. *Nature*, **426**, 645–647.
- RITTENHOUSE, G. (1943) The transportation and deposition of heavy minerals. *Geol. Soc. Am. Bull.*, **54**, 1725–1780.

- RUBEY, W.W. (1933) The size distribution of heavy minerals in a water-lain sandstone. *J. Sediment. Petrol.*, **3**, 3–29.
- SAMBRIDGE, M.S. & COMPSTON, W. (1994) Mixture modeling of multi component data sets with application to ion-probe zircon ages. *Earth Planet. Sci. Lett.*, **128**, 373–390.
- SEARLE, M.P. & GODIN, L. (2003) The South Tibetan detachment and the Manaslu Leucogranite; a structural reinterpretation and restoration of the Annapurna–Manaslu Himalaya, Nepal. *J. Geol.*, **111**, 505–523.
- SHESKIN, D. (2003) *Handbook of Parametric and Nonparametric Statistical Procedures*, 3rd edn. Chapman & Hall/CRC, Boca Raton, FL.
- SHIDELER, G.L. & FLORES, R.M. (1980) Heavy-mineral variability in fluvial sediments of the lower Rio Grande, southwestern Texas. *Texas J. Sci.*, **32**, 73–91.
- SLINGERLAND, R. (1977) The effect of entrainment on the hydraulic equivalence relationships of light and heavy minerals in sands. *J. Sediment. Petrol.*, **47**, 753–770.
- SLINGERLAND, R.L. (1984) The role of hydraulic sorting in the origin of fluvial placers. *J. Sediment. Petrol.*, **54**, 137–150.
- SMALE, D. (1990) Distribution and provenance of heavy minerals in the South Island: a review. *N. Zeal. J. Geol. Geophys.*, **33**, 557–571.
- SPIEGEL, C., SIEBEL, W., KUHELMANN, J. & FRISCH, W. (2004) Toward a comprehensive provenance analysis: a multi-method approach and its implications for the evolution of the Central Alps. In: *Detrital Thermochronology – Provenance Analysis, Exhumation and Landscape Evolution of Mountain Belts* (Ed. by M. Bernet & C. Spiegel) Geological Society of America Special Publication, Boulder, CO, **378**, 37–50.
- SUROUR, A.A., EL-KAMMAR, A.A., ARAFA, E.H. & KORANY, H.M. (2003) Dahab stream sediments, southeastern Sinai, Egypt: a potential source of gold, magnetite and zircon. *J. Geochem. Expl.*, **77**, 25–43.
- TURNAU-MORAWSKA, M. (1984) Importance of heavy mineral analysis in solving geological problems. In: *Stability of Heavy Minerals in Sediments*, 1st edn (Ed. by G. Luepke), pp. 280–287. Van Nostrand Reinhold, New York.
- UPRETI, B.N. (1999) An overview of the stratigraphy and tectonics of the Nepal Himalaya. *J. Asian Earth Sci.*, **17**, 577–606.
- VANCE, D., BICKLE, M., IVY-OCHS, S. & KUBIK, P.W. (2003) Erosion and exhumation in the Himalaya from cosmogenic isotope inventories of river sediments. *Earth Planet. Sci. Lett.*, **206**, 273–288.
- WOBUS, C., HODGES, K.V. & WHIPPLE, K.X. (2003) Has focused denudation sustained active thrusting at the Himalayan topographic front. *Geology*, **31**, 861–864.

Manuscript accepted 7 October 2005